Heavy-flavour spectra in high energy nucleus-nucleus collisions

W.M. Alberico[1,2], A. Beraudo[1,2,3,4], A. De Pace[2], A. Molinari[1,2], M. Monteno[2], M. Nardi[2], and F. Prino[2]

[1] Dipartimento di Fisica Teorica dell'Università di Torino, via P.Giuria 1, I-10125 Torino, Italy
[2] Istituto Nazionale di Fisica Nucleare, Sezione di Torino, via P.Giuria 1, I-10125 Torino, Italy
[3] Centro Studi e Ricerche *Enrico Fermi*, Piazza del Viminale 1, Roma, Italy
[4] Physics Department, Theory Unit, CERN, CH-1211 Genève 23, Switzerland

Abstract. The propagation of the heavy quarks produced in relativistic nucleus-nucleus collisions at RHIC and LHC is studied within the framework of Langevin dynamics in the background of an expanding deconfined medium described by ideal and viscous hydrodynamics. The transport coefficients entering into the relativistic Langevin equation are evaluated by matching the hard-thermal-loop result for soft collisions with a perturbative QCD calculation for hard scatterings. The heavy-quark spectra thus obtained are employed to compute the differential cross sections, the nuclear modification factors R_{AA} and the elliptic flow coefficients v_2 of electrons from heavy-flavour decay.

1 Introduction

The aim of the ongoing heavy ion programme at RHIC (with Au-Au collisions at $\sqrt{s}_{\rm NN}$ up to 200 GeV) and of the recently started programme at LHC (with the first Pb-Pb collisions at $\sqrt{s}_{\rm NN} = 2.76$ TeV) is the creation of a deconfined system of quarks and gluons, with a lifetime sufficiently long (a few fm) to allow measurable signals to show up. The challenge is not only to establish the formation of the deconfined phase, but also to study the properties of the produced medium. Among the most interesting observables investigated at RHIC, perhaps, there are the quenching of high-p_T hadron spectra, expressed through the *nuclear modification factor* $R_{\rm AA}(p_T)$ [1,2], and the azimuthal anisotropy of particle emission in the transverse plane, quantified by the *elliptic-flow coefficient* v_2 [3,4]. The asymptotic value $R_{\rm AA}(p_T) \approx 0.2$ found at high p_T indicates that the matter created in the heavy ion collisions is very opaque, leading to a sizable energy loss of the few high-momentum partons produced in the initial instants of the collisions by hard processes. The latter are describable in the framework of perturbative Quantum Chromodynamics (pQCD). Furthermore, the elliptic flow observed in semi-central collisions seems to find a natural explanation within a hydrodynamical description of the medium, displaying an expansion driven by the pressure gradient: the latter, resulting larger along the reaction plane, leads to the azimuthal anisotropy of the transverse-momentum spectra. Notably, the large value of v_2 found in the data, besides supporting the hydrodynamical behavior of the created matter (entailing a mean free path $\lambda_{\rm mfp}$ much smaller then the system size L), requires also a quite short thermalization time ($\tau_0 \lesssim 1$ fm). R_{AA} and v_2 have recently been measured also by the ALICE detector at LHC for unidentified particles [5,6].

These two observables ($R_{\rm AA}$ an v_2) have been initially studied for the case of light-flavour hadrons (pions, kaons, protons, ...), arising from the hadronization of gluons and light quarks. In this context, the quenching of hadron spectra has been attributed to the energy-loss of hard partons due to the radiation of soft gluons ($\omega \ll E_{\rm hard}$) occurring in the presence of scattering centers (the plasma particles). Different theoretical approaches have been proposed [7,8,9,10], all stressing the importance of coherence (Landau-Pomeranchuk [11] and Migdal [12]) effects for large enough formation times of the emitted gluon, so that $\tau_{\rm form} \gtrsim \lambda_{\rm mfp}$.

If the soft-gluon radiation were the only mechanism responsible for energy loss, one would expect heavy quarks (c and b) to be much less quenched. Characteristic effects occurring for massive particles are the suppression of collinear gluon emission for angles $\theta \lesssim M/E$ (*dead cone effect* [13,14]), the shortening of the gluon formation time and the suppression of the radiated gluon spectra at large energy [15]. Furthermore, while light-hadron spectra get contribution from the fragmentation of partons belonging both to the fundamental (quarks) and the adjoint (gluons) representations, heavy-flavour electrons arise only from the decays of c and b quarks. Hence, the associated Casimir factor C_F (smaller then C_A of the gluons) should entail a larger mean-free-path, resulting in a lower rate of gluon radiation. However, single-electron spectra (resulting from the semi-leptonic decays of D and B mesons) measured by the PHENIX experiment at RHIC show a similar level of suppression as the one found for light hadrons [16,17] (a similar analysis is being performed by the STAR collaboration); moreover, they also display a sizable elliptic flow.

These findings hint at reconsidering the importance of collisional energy loss. Calculations of the stopping power of the quark-gluon plasma (QGP) for heavy quarks due to elastic collisions can be found for instance in Refs. [18,19, 20].

An appropriate tool to study the final spectra of heavy quarks, after their evolution in the fireball created in the heavy ion collisions, is given by the (relativistic) Langevin equation, which relies on the picture of many uncorrelated random collisions [21,22]. This approach — pursued by solving either the Langevin equation or the corresponding Fokker-Planck equation — has already been explored in the literature [23,24,25,26,27,28] and will be the one addressed in this paper. Solving the Langevin equation requires as an input the knowledge of a few transport coefficients, accounting for the interaction of the heavy quarks with the medium: indeed, in this framework, the latter gives rise to a friction force and a momentum broadening. The various calculations available in the literature [23,24,25,26,27,28] differ mainly in the way they estimate the above coefficients, either inspired by pQCD or within less conventional scenarios (assuming for instance the existence of resonant states in the plasma [24] or the AdS/CFT correspondence [26]). In all the cases the freedom of tuning some parameter allows one to explore more/less strongly coupled regimes.

However, before looking for alternative explanations, it appears important to have at hand a fully consistent weakly coupled calculation, to check how closely the experimental data can be reproduced within a perturbative picture and how much room is left for more "exotic" scenarios. This is the major goal of our paper, in which we provide a microscopic evaluation of the heavy-quark transport coefficients and we use them to solve the Langevin equation for c and b quarks that are produced in nucleus-nucleus collisions and are let propagate randomly in the resulting deconfined medium. Our calculation relies on the separate treatment of soft and hard collisions. The first ones, mediated by the exchange of long wavelength gluons, will be described within the Hard Thermal Loop (HTL) approximation, which resums medium effects. Hard collisions, involving a high-momentum exchange, will be calculated in kinetic theory, employing leading order pQCD matrix elements [29]. The two contributions will then be summed up. Once the transport coefficients have been calculated, we can address the numerical solution of the Langevin equation, given suitable initial conditions and a background medium.

The initial heavy-quark pairs are produced using the POWHEG package [30,31], a hard event generator for heavy-quark production in hadronic collisions, which implements pQCD at next-to-leading order (NLO). Since it generates events, this code is particularly suitable for a Langevin simulation. Care is taken to allow also for shadowing and transverse momentum broadening effects. Once created, the heavy quark is allowed to propagate in the hot medium according to the Langevin dynamics, with transport coefficients calculated as mentioned above. The evolution of the background medium is described by two different scenarios, namely ideal [32,33,34] and viscous [35,36,37] hydrodynamics, in order to estimate the dependence of our results on the hydrodynamical scheme. Around the phase transition energy density the c and b quarks are made hadronize (at the moment, for the sake of simplicity, only through fragmentation) and then decay to electrons, to allow for a comparison with the existing experimental data from RHIC for open heavy-flavour electrons. Results will be presented for the invariant yields, the nuclear modification factors and the elliptic flow coefficients at the kinematics of both RHIC and LHC. For the latter we have chosen the highest center-of-mass energy that the heavy ion experiments should be able to reach, i. e. $\sqrt{s} = 5.5$ TeV. Preliminary results have already been presented in Refs. [38].

Table 1. Total production cross sections for heavy-quark pairs calculated with POWHEG for pp collisions at two different center-of-mass energies and for two choices of PDF's: CTEQ6M alone (suitable for bare pp collisions) and supplemented by the EPS09 nuclear modifications [39] (for NN events embedded in a nucleus-nucleus collision).

	$\sigma_{c\bar{c}}$ (mb) per NN event		$\sigma_{b\bar{b}}$ (mb) per NN event	
$\sqrt{s}$	CTEQ6M	(+EPS09)	CTEQ6M	(+EPS09)
200 GeV	0.254	0.236	1.77×10^{-3}	2.03×10^{-3}
5.5 TeV	3.015	2.288	0.187	0.169

Our paper is organized as follows: in Sect. 2 we introduce the theoretical tools employed in generating the heavy-quark spectra after a high-energy heavy ion collision, examining all the steps of the process, from the production stage, through the hydrodynamic evolution, the Langevin propagation, the calculation of the transport coefficients, up to hadronization and decay; in Sect. 3 we present and discuss our findings for the differential spectra, the nuclear modification factor and the elliptic-flow coefficient; finally, in Sect. 4 we sum up our conclusions; some more technical material is deferred to the Appendices.

2 Theoretical framework

2.1 Heavy-quark production in pp and AA collisions

For every experimental setup (either pp or AA at $\sqrt{s} =$ 200 GeV (RHIC) and $\sqrt{s} = 5.5$ TeV (LHC)) we have generated 4.5×10^7 heavy-quark pairs (either $c\bar{c}$ or $b\bar{b}$) using the POWHEG event generator [30,31], which implements pQCD at NLO.

There is considerable uncertainty in the $Q\bar{Q}$ production cross section, due to uncertainties in the quark masses and in the renormalization and factorization scales. Here we have chosen $m_c = 1.5$ GeV, $m_b = 4.8$ GeV and for the values of the renormalization and factorization scales we have kept the default choice in POWHEG, that is the heavy-quark transverse mass in the $Q\bar{Q}$ reference frame [30]. For pp events we have employed the CTEQ6M parton

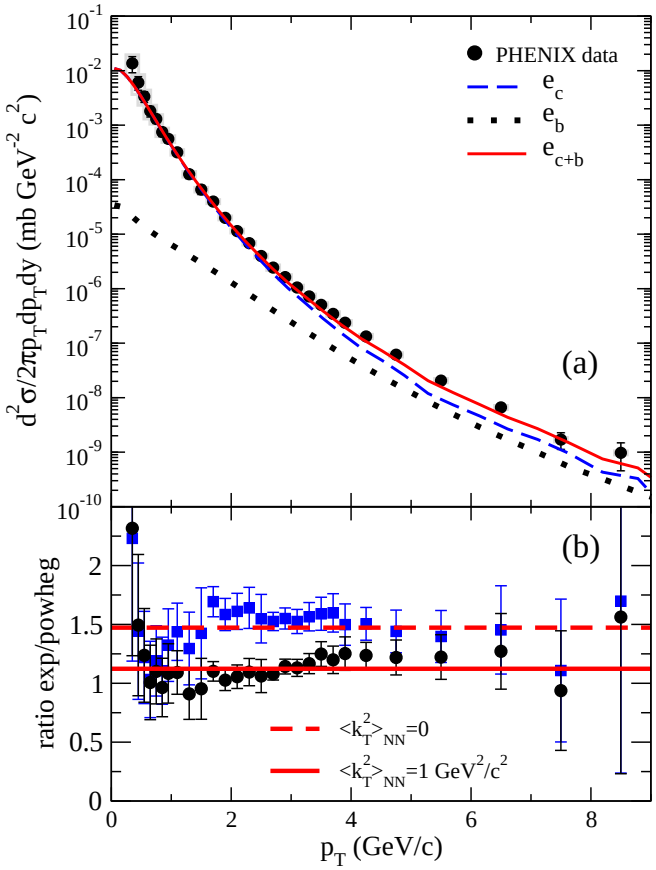

Fig. 1. (a) Invariant differential cross section of electrons $[(e^+ + e^-)/2]$, from heavy-flavour decay in pp collisions at $\sqrt{s} = 200$ GeV, at mid-rapidity as a function of transverse momentum. The experimental points represent PHENIX data [42, 17]; both statistical (error bars) and systematic (gray boxes) errors are displayed. The curves represent the contributions coming from electrons originating from a charm or bottom quark generated by POWHEG with inclusion of transverse broadening. (b) ratio of data to the POWHEG prediction as a function of p_T, with (circle) and without (square) inclusion of transverse broadening; the lines represent the best fit to a constant.

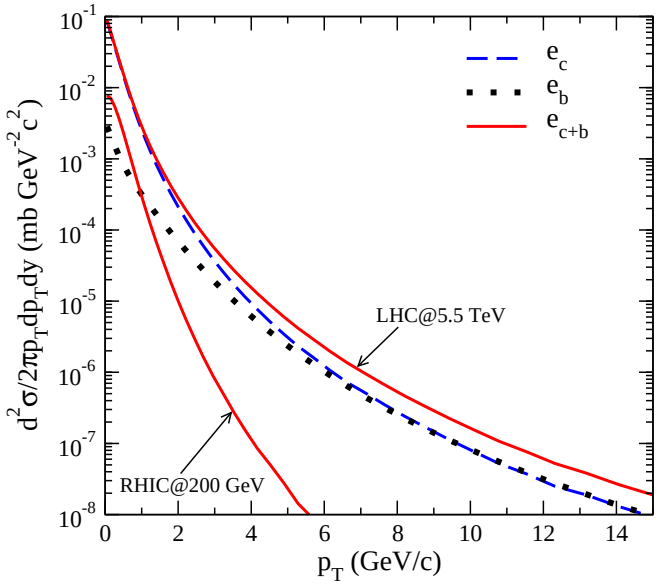

Fig. 2. Invariant differential cross section of electrons $[(e^+ + e^-)/2]$, from heavy-flavour decay in pp collisions at $\sqrt{s} = 5.5$ TeV, at mid-rapidity as a function of transverse momentum. The curves represent the contributions coming from electrons originating from a charm or bottom quark generated by POWHEG with inclusion of transverse broadening. For comparison we have also included the total yield of electrons at RHIC from Fig. 1.

distribution function (PDF). The total $c\bar{c}$ and $b\bar{b}$ production cross sections one gets at RHIC energies (see Table 1) are very close to the central values predicted by FONLL [40]. Another important effect to be accounted for in the production cross sections is related to the intrinsic transverse momentum of the initial partons. We have adopted the procedure described in Ref. [41], which amounts to add to the out-coming heavy quarks a transverse momentum contribution randomly generated from a Gaussian distribution with given variance $\langle k_T^2 \rangle_{\rm NN}$. For pp collisions we have adopted the standard value $\langle k_T^2 \rangle_{\rm NN} = 1$ GeV^2/c^2.

In Fig. 1 one can see the invariant differential cross sections of electrons from heavy-flavour decay (see Sect. 2.5 for details about hadronization and decay) in pp collisions at $\sqrt{s} = 200$ GeV, compared to the mid-rapidity data from PHENIX [42,17][1]. One observes that the pQCD outcome provides a fairly good description of both the shape and the absolute magnitude of the data. In panel (b) of the figure the ratio between experiment and theory is also displayed: this ratio is nearly p_T-independent and a best fit with a constant provides for the latter the value 1.12. Given a 10% normalization uncertainty in the data (not shown in the figure) and the previously mentioned uncertainties on the theoretical parameters, a 12% difference between theory and data can be easily accommodated. Accordingly, for sake of simplicity, in the following we have chosen to multiply by this factor all the calculated cross sections at RHIC energies (of course, R_{AA} and v_2 are not affected by cross section normalization). In Fig. 1b we also display the ratio of data to the cross section generated without any transverse momentum broadening: in this case the discrepancy is fairly larger (although still within the experimental and theoretical uncertainties).

In Fig. 2 the invariant differential cross sections of electrons from heavy-flavour decay in pp collisions at $\sqrt{s} = 5.5$ TeV are reported: apart from the much larger strength and the less steep slope of the cross sections, one observes

[1] For the purpose of comparing to the PHENIX data, the doubly differential cross sections have been calculated by integrating over the experimental acceptance in pseudo-rapidity ($|\eta| < 0.35$) and dividing by the rapidity range ($\Delta y \cong 0.7$). For consistency, also the cross sections at the energy of LHC have been calculated in the same way, using the constraints of the ALICE experiment ($|\eta| < 0.9$ and $\Delta y \cong 1.8$).

that the bottom relative contribution is much more important than at the RHIC energy.

In the case of nucleus-nucleus collisions, there are two important differences one has to consider in connection to the initial heavy-quark distributions. First of all, the nuclear PDF's should be different from the ones employed in *pp* collisions and, to account for this occurrence, we have adopted here the EPS09 scheme [39]. In principle, the density probed by the colliding partons should depend on the impact parameter b: in describing nucleus-nucleus collisions we have made the simple choice of employing the EPS09 scheme for impact parameters $b < 2R$ and of neglecting nuclear corrections for $b > 2R$ (R being the radius of the nuclear density distribution). The main consequence of using a different PDF in AA and pp collisions relates to the different total (per binary collision) $c\bar{c}$ and $b\bar{b}$ production cross sections one gets, as one can see in Table 1. Indeed, since in a binary process the longitudinal momentum fraction carried by the two initial partons (most of the times gluons) is given by [43]

$$x_{1/2} = M_{Q\bar{Q}}/\sqrt{s}_{\rm NN} e^{\pm y_{Q\bar{Q}}}, \qquad (1)$$

$M_{Q\bar{Q}}$ and $y_{Q\bar{Q}}$ being the invariant mass and rapidity of the $Q\bar{Q}$ pair, one can get larger or smaller cross sections in AA collisions, at different energies and quark masses, depending upon whether one is probing the anti-shadowing or shadowing regions. For instance, at RHIC energy, because of the large bottom mass, the main contributions come from relatively large values of x, where anti-shadowing dominates — hence a larger $b\bar{b}$ cross section per binary collision results — whereas at LHC energies one is mainly probing the low x shadowing region, yielding smaller cross sections. This fact has sizable consequences on R_{AA}, as we shall see later.

A second difference one has to cope with in AA collisions concerns the larger transverse momentum acquired on average by the colliding partons, because of the large size of the traversed medium. To get a realistic estimate for $\langle k_T^2 \rangle_{AA}$ in nucleus-nucleus collisions we have adopted a Glauber approach — developed in Refs. [44,45] in order to study the p_T distribution of charmonia produced in proton-nucleus and nucleus-nucleus collisions [46] — and we have generalized it to study the inclusive single-quark spectra. Details of the procedure can be found in Appendix A. One gets an average squared transverse momentum that depends not only on the impact parameter of the collision and on the nuclei involved, but also on the transverse position of the $Q\bar{Q}$ pair. To get an orientation on the magnitude of the quantities involved, we mention that at RHIC energy one gets, depending upon the impact parameter, average values of $\langle k_T^2 \rangle_{AA}$ around $1.3 \div 1.5$ GeV^2/c^2 for charm and around $1.8 \div 2.3$ GeV^2/c^2 for bottom in Au-Au collisions; at the LHC ($\sqrt{s} = 5.5$ TeV) around $1.5 \div 1.8$ GeV^2/c^2 for charm and around $2.5 \div 3.3$ GeV^2/c^2 for bottom in Pb-Pb collisions.

Finally, for AA collisions, since we are following in the Langevin framework the space-time propagation of an ensemble of heavy quarks, we have also to specify their space-time distribution at the onset of the hydrodynamical evolution of the background medium. This we do consistently with the choice discussed below for the initial conditions of the hydrodynamic equations. Namely, at the initial proper time τ_0 the position of the heavy quarks in the transverse plane is calculated in a Glauber framework according to a distribution generated by the nuclear overlap function $T(x + b/2, y)T(x - b/2, y)$, where

$$T(x, y) = \int dz\, \rho(x, y, z), \qquad (2)$$

ρ being a Fermi parameterization of the nuclear density [47] and b the impact parameter. In the longitudinal direction we set $z = \tau_0 \sinh \eta_s$, with

$$\eta_s \equiv \frac{1}{2} \ln \frac{t + z}{t - z} = \frac{1}{2} \ln \frac{E + p_z}{E - p_z}. \qquad (3)$$

2.2 Hydrodynamic evolution at RHIC and LHC

Hydrodynamics has been successfully applied to the description of collective phenomena in heavy ion collisions at RHIC, yielding a sensible description for a number of experimental observables. For our purposes, hydrodynamics provides the full space-time evolution of the properties of the expanding medium — such as temperature, flow velocity and energy density — that are needed to follow the propagation of the heavy quarks. We have chosen two different implementations of the relativistic hydrodynamic equations, whose codes are publicly available, namely ideal [32,33,34] and viscous [35,36,37] hydrodynamics, both assuming exact longitudinal boost invariance. The two models differ not only in the ideal/viscous implementation (with the ratio of shear viscosity to entropy density taken to be $\eta/s = 0.08$ in the viscous case), but also in the choice of the equation of state (EOS) and of the initial conditions. By comparing the results obtained in the two scenarios one can get an estimate of the amount of uncertainty due to the treatment of the background medium.

The initial energy density distribution is computed in both cases according to the Glauber model, using either the number of participating nucleons ($N_{\rm part}$) or the number of binary collisions ($N_{\rm coll}$). In the ideal model [32] the distribution has been ascribed for the 75% to "soft"

Table 2. Values of the initial proper time τ_0, central entropy density s_0 and central temperature T_0 employed as initial conditions for the hydrodynamical evolution.

	$\eta/s = 0$			$\eta/s = 0.08$		
	τ_0 (fm)	s_0 (fm^{-3})	T_0 (MeV)	τ_0 (fm)	s_0 (fm^{-3})	T_0 (MeV)
RHIC	0.6	110	357	0.1	840	666
				0.6	140	387
				1	84	333
LHC	0.1	2438	1000	0.1	1840	854
	0.45	271	482	1	184	420

processes scaling as $N_{\rm part}$ and for the 25% to "hard" processes scaling as $N_{\rm coll}$; in the viscous model the initial energy density is proportional to $N_{\rm coll}$. Concerning the EOS, in the ideal case it is obtained by matching, through a Maxwell construction, a gas of hadron resonances with an ideal gas of massless quarks and gluons; this model yields a first order transition at $T_{\rm crit} = 164$ MeV. In the viscous case, one employs the more realistic EOS of Ref. [48], which implements a crossover between a low temperature hadron-resonance gas and a high temperature pQCD calculation.

The initial proper time τ_0 is one of the parameters of the hydrodynamical model: at the conditions of RHIC, the values $\tau_0 = 0.6$ fm and $\tau_0 = 1$ fm have been chosen by the authors in the ideal [32] and viscous [36] cases, respectively. Since the value of τ_0 has some impact on the final heavy quark spectra (a lower value provides a longer propagation and exposes the heavy quark to higher temperatures), we have also explored a scenario with a very small value of τ_0, by adjusting the maximal initial entropy density s_0 (hence, through the EOS, the corresponding initial energy density) in such a way to maintain the same particle density, using the relation

$$\frac{dN}{dy} \sim s_0 \tau_0. \tag{4}$$

At the LHC regime, on the other hand, a full experimental constraint is not available yet (although first data on particle density at mid-rapidity are becoming available at $\sqrt{s} = 2.76$ TeV [49]). Here we have followed Refs. [50, 51] (ideal) and Ref. [37] (viscous), where the initial conditions have been fixed in order to match, instead of the experimentally observed multiplicities, the range of the predicted ones. Our set of initial conditions is summed up in Table 2.

As an example of the differences among the various hydrodynamical scenarios that we have employed, in Fig. 3 we display the temperature and the energy density at the center of the fireball during the hydrodynamical evolution for a few cases of semi-peripheral collisions. For every experimental setup, at RHIC and LHC, we have reported the scenarios giving rise to the lowest and to the highest temperatures attained during the evolution.

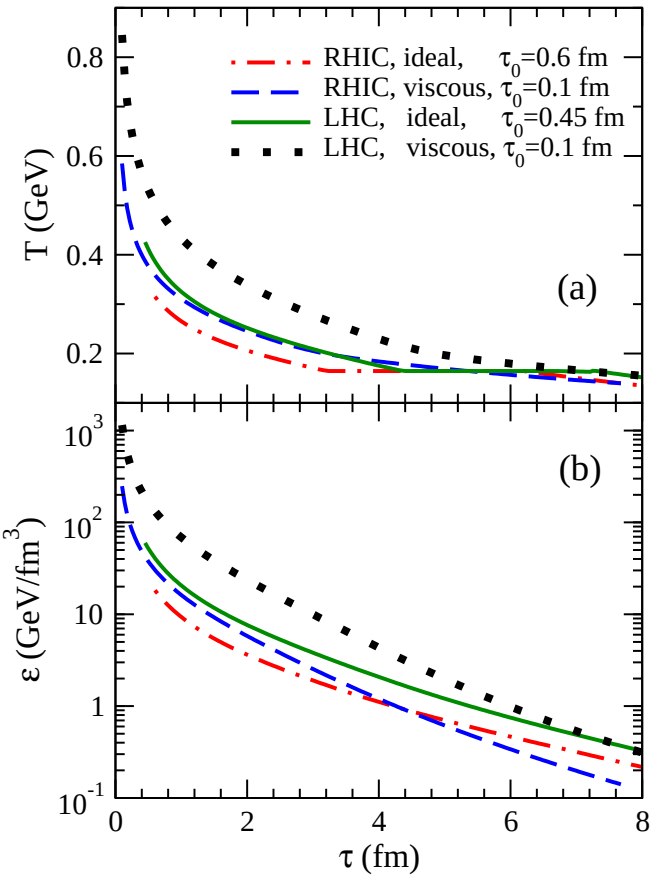

Fig. 3. (a) The temperature at the center of the fireball during hydrodynamical evolution for a few scenarios both at RHIC (impact parameter $b = 8.44$ fm) and LHC ($b = 8.77$ fm). (b) The energy density at the center of the fireball during hydrodynamical evolution for the same scenarios.

2.3 Langevin dynamics in a relativistic fluid

We wish to follow the propagation of c and b quarks — initially produced in hard pQCD processes — in the expanding, thermalized fireball of deconfined matter that one expects to arise from a high energy heavy ion collision. The propagation of the heavy quarks in such a hot environment is modeled as a Brownian motion by employing a relativistic Langevin equation [21,23,24,26]: our implementation of the model has been discussed in detail in a previous paper [22], where we dealt with the simpler case of a static homogeneous medium at rest. Here, we briefly summarize the essential points of model.

The evolution with time of the momentum of a relativistic Brownian particle is provided by the Langevin equation:

$$\frac{d\boldsymbol{p}}{dt} = -\eta_D(p)\boldsymbol{p} + \boldsymbol{\xi}(t), \tag{5}$$

where the *drag coefficient* $\eta_D(p)$ describes the deterministic friction force acting on the heavy quark, whereas the term $\boldsymbol{\xi}$ accounts for the random collisions with the constituents of the medium. The effect of the stochastic term is completely determined once its temporal correlation function is fixed. The latter is usually assumed to be given by

$$\langle \xi^i(t)\xi^j(t')\rangle = b^{ij}(\boldsymbol{p})\delta(t-t'), \tag{6}$$

entailing that collisions at different time-steps are uncorrelated. The tensor $b^{ij}(\boldsymbol{p})$ can be decomposed with a standard procedure according to

$$b^{ij}(\boldsymbol{p}) \equiv \kappa_L(p)\hat{p}^i\hat{p}^j + \kappa_T(p)(\delta^{ij} - \hat{p}^i\hat{p}^j) \tag{7}$$

in terms of the coefficients $\kappa_{L/T}(p)$, which represent the squared longitudinal/transverse momentum per unit time exchanged by the quark with the medium. It is useful to

introduce the related tensor

$$g^{ij}(\boldsymbol{p}) \equiv \sqrt{\kappa_L(p)}\hat{p}^i\hat{p}^j + \sqrt{\kappa_T(p)}(\delta^{ij} - \hat{p}^i\hat{p}^j) \equiv g_L(p)\hat{p}^i\hat{p}^j + g_T(p)(\delta^{ij} - \hat{p}^i\hat{p}^j), \quad (8)$$

which allows one to factor out the momentum dependence of the noise term in Eq. (5), thus obtaining the equation

$$\frac{dp^i}{dt} = -\eta_D(p)p^i + g^{ij}(\boldsymbol{p})\eta^j(t), \quad (9)$$

with

$$\langle \eta^i(t)\eta^j(t')\rangle = \delta^{ij}\delta(t-t'). \quad (10)$$

Finally, the drag coefficient $\eta_D(p)$ is fixed in order to ensure the approach to equilibrium: for large times the momenta of an ensemble of heavy quarks should be described by an equilibrium Maxwell-Jüttner distribution. Actually, the whole procedure depends on the discretization scheme employed in the numerical solution of Eq. (9), which belongs to the class of the *stochastic differential equations* [52,53]. In the Ito discretization scheme one gets:

$$\eta_D^{\rm Ito}(p) \equiv \frac{\kappa_L(p)}{2TE} - \frac{1}{E^2}\left[(1-v^2)\frac{\partial\kappa_L(p)}{\partial v^2} + \frac{\kappa_L(p)-\kappa_T(p)}{v^2}\right], \quad (11)$$

where v is the quark velocity, E its energy and T the medium temperature.

The set of Eqs. (8-11) is defined in the rest frame of the background medium and it allows one to study the quark propagation once the transport coefficients are given. These depend on the medium temperature, which in turn, in the expanding fireball, depends on the space-time position occupied by the heavy quark. Hence, to study the fate of a heavy quark through the quark-gluon plasma, we adopt the following procedure:

- We determine the initial four-momentum p^μ and the initial space-time position x^μ of the heavy quark (in the laboratory system) as explained in Sect. 2.1.
- Given the position x^μ, we use the information from the hydrodynamic simulation (Sect. 2.2) to obtain the fluid local temperature $T(x)$, velocity $u^\mu(x)$ and energy density $\varepsilon(x)$.
- We check (see Sect. 2.5) whether the conditions for hadronization apply: in this case the procedure is ended; otherwise
- we make a Lorentz transformation ($p^\mu \to \bar{p}^\mu$) to the fluid rest frame, employ Eqs. (8-11) to update the quark momentum ($\bar{p}^\mu \to \bar{p}'^\mu$) and boost it back to the laboratory ($\bar{p}'^\mu \to p'^\mu$).
- We update the space-time step made by the quark in the rest frame ($\Delta\bar{x}^\mu = (\bar{p}^\mu/E_{\bar{p}})\Delta\bar{t}$), boost it to the laboratory ($\Delta\bar{x}^\mu \to \Delta x^\mu$) and use it to update the quark position ($x^\mu \to x'^\mu$).
- Given the new momentum p'^μ and the new position x'^μ the procedure is started again until the conditions for hadronization are met.

The time step in the rest frame, which enters in updating the quark position and also the quark momentum through the Langevin equation, in our calculations has the value $\Delta\bar{t} = 0.02$ fm.

2.4 Heavy-quark transport coefficients

In the approach to stochastic dynamics based on the (relativistic) Langevin equation, the information on the properties of the medium crossed by a Brownian particle is encoded in the drag and momentum-diffusion coefficients η_D and $\kappa_{T/L}$. Following the random motion of the heavy quarks in the QGP requires then the calculation of the above coefficients, starting from the microscopic theory, i.e. finite temperature QCD. In accord with Refs. [19,20], we accomplish this task by separating soft and hard collisions depending upon the value of the Mandelstam variable $t \equiv \omega^2 - q^2$ that characterizes the elementary scattering, and summing at the end the two contributions[2].

Soft scatterings — corresponding to $\sqrt{|t|} \sim gT$ — occur quite frequently, with a typical mean free path $\lambda_{\rm mfp}^{\rm soft} \sim 1/g^2T$. Being related to the exchange of long-wavelength gluons, they require a careful treatment of medium effects, which can be achieved by describing these soft collisions within the HTL approximation. Hard scatterings — corresponding to $\sqrt{|t|} \gtrsim T$ — are more rare, the mean free path being in this case $\lambda_{\rm mfp}^{\rm hard} \sim 1/g^4T$, but, since they cause a sizable momentum exchange, their contribution to the transport coefficients is substantial and will be evaluated, as already mentioned, within a microscopic kinetic calculation based on pQCD. We set $|t|^* \sim m_D^2$, m_D being the Debye mass, as the intermediate cutoff. Clearly, the final results should not be too much affected by the choice of $|t|^*$ and we have verified that this is actually the case, even for temperatures of experimental interest, where the coupling is not really small.

The coupling constant g has been chosen to run according to the two-loop QCD beta-function, with $\Lambda_{\rm QCD} = 261$ MeV, as in Ref. [54]. The coupling constant displays a strong dependence on the unknown value of the temperature dependent scale $\mu \propto T$ and this has important consequences on the final observables, as we shall see in the following. To shed light on this important issue, we shall explore the effect on the calculated quantities for a wide range of values, $\pi T \le \mu \le 2\pi T$.

2.4.1 Soft collisions: hard thermal loops

The contribution of soft collisions to the transport coefficients has already been obtained in our previous work [22], to which we refer for details. However, due to our choice of setting $|t|^*$ as an intermediate cutoff, it is necessary to rewrite the formulas in Ref. [22] for $\kappa_{T/L}$ employing $|t| \equiv q^2 - \omega^2$ and $x \equiv \omega/q$ as integration variables. One gets:

$$\kappa_T^{\rm soft} = \frac{C_F g^2}{8\pi^2 v}\int_0^{|t|^*} d|t| \int_0^v dx \frac{|t|^{3/2}}{2(1-x^2)^{5/2}}\overline{\rho}(|t|,x)$$

[2] Note that this differs from what is usually done in the literature (see, e.g., Ref. [18]), where the separation between hard and soft scatterings is related to the spatial momentum q exchanged in the collision.

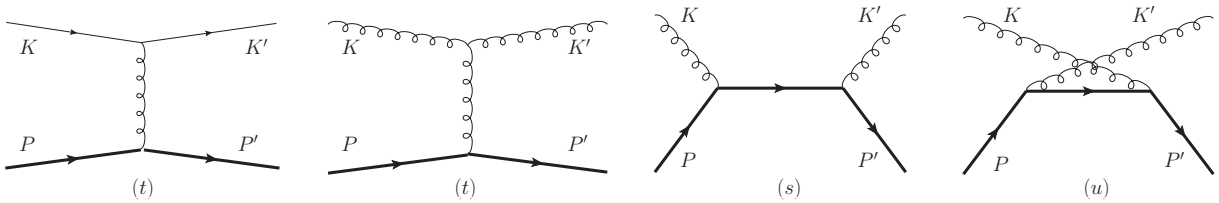

Fig. 4. The tree level diagrams for the hard scattering of a heavy quark off a light (anti-)quark of the thermal bath and for the hard scattering (in the t, s and u channels) of a heavy quark off a gluon.

$$\times\left(1-\frac{x^2}{v^2}\right)\coth\left(\frac{x\sqrt{|t|/(1-x^2)}}{2T}\right) \quad (12)$$

and

$$\kappa_L^{\rm soft}=\frac{C_F g^2}{4\pi^2 v}\int_0^{|t|^*}d|t|\int_0^v dx\frac{|t|^{3/2}}{2(1-x^2)^{5/2}}\overline{\rho}(|t|,x) \times\frac{x^2}{v^2}\coth\left(\frac{x\sqrt{|t|/(1-x^2)}}{2T}\right), \quad (13)$$

for the transverse and longitudinal momentum diffusion coefficients, respectively. In the above, v is the quark velocity, $C_F=4/3$ the quark Casimir factor and

$$\overline{\rho}(|t|,x)\equiv\rho_L(|t|,x)+(v^2-x^2)\rho_T(|t|,x), \quad (14)$$

where $\rho_{L/T}$ are the continuum parts of the HTL gluon spectral functions:

$$\rho_L(|t|,x)=\pi m_D^2 x\left\{\left[\frac{|t|}{1-x^2} +m_D^2\left(1-\frac{x}{2}\ln\left|\frac{x+1}{x-1}\right|\right)\right]^2+\left[\pi m_D^2\frac{x}{2}\right]^2\right\}^{-1}$$
$$\rho_T(|t|,x)=\pi m_D^2\frac{x}{2}(1-x^2)\left\{\left[|t|+m_D^2\frac{x}{2}\right. \right. \quad (15)$$
$$\left.\left.\times\left(1+\frac{1-x^2}{2x}\ln\left|\frac{x+1}{x-1}\right|\right)\right]^2+\left[\frac{\pi}{2}m_D^2\frac{x}{2}(1-x^2)\right]^2\right\}^{-1}.$$

2.4.2 Hard collisions: perturbative QCD

The contribution from hard collisions to the transport coefficients $\kappa_{T/L}$ can be calculated starting from their microscopic definition, namely

$$\kappa_T\equiv\frac{1}{2}\left\langle\frac{\Delta q_T^2}{\Delta t}\right\rangle \quad\text{and}\quad \kappa_L\equiv\left\langle\frac{\Delta q_L^2}{\Delta t}\right\rangle, \quad (16)$$

and by weighting the interaction rate with the squared transverse and longitudinal momentum exchanged in the collisions with gluons and (anti-)quarks of the medium. One has

$$\kappa_{T/L}^{\rm hard}=\kappa_{T/L}^g+\kappa_{T/L}^q, \quad (17)$$

where (employing the notation $\int_k\equiv\int d\boldsymbol{k}/(2\pi)^3$)

$$\kappa_T^{g/q}=\frac{1}{2E}\int_k\frac{n_{B/F}(k)}{2k}\int_{k'}\frac{1\pm n_{B/F}(k')}{2k'}\int_{p'}\frac{\theta(|t|-|t|^*)}{2E'} \times(2\pi)^4\delta^{(4)}(P+K-P'-K')\left|\overline{\mathcal{M}}_{g/q}(s,t)\right|^2\frac{q_T^2}{2} \quad (18)$$

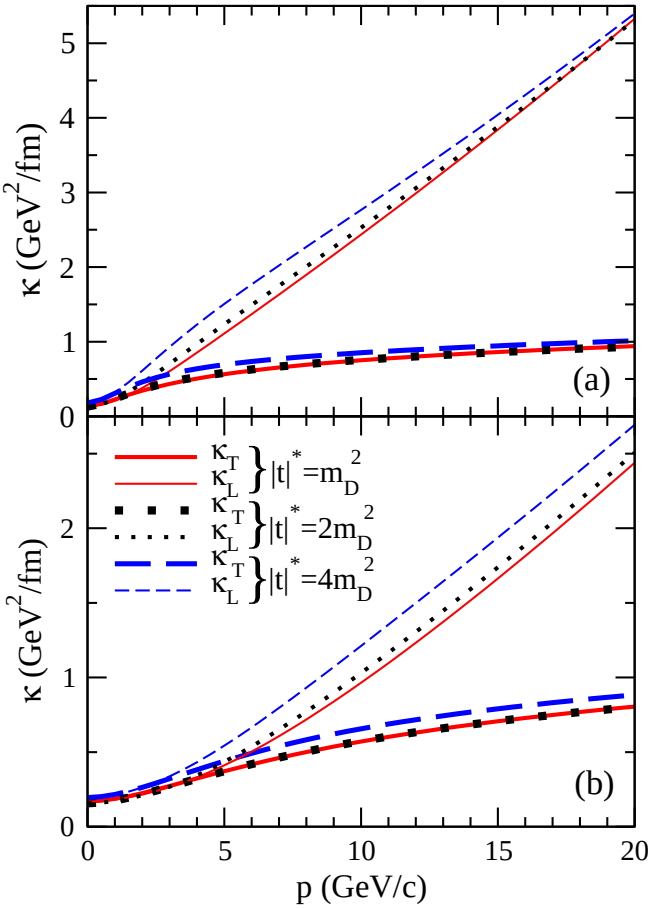

Fig. 5. The charm (upper panel) and bottom (lower panel) momentum diffusion coefficients $\kappa_{T/L}(p)$ resulting from the sum of the soft and hard contributions. The sensitivity to the intermediate cutoff $|t|^*\sim m_D^2$ is very mild. The curves refer to the temperature $T=400$ MeV, with the coupling g evaluated at the scale $\mu=(3/2)\pi T$.

and

$$\kappa_L^{g/q} = \frac{1}{2E}\int_k \frac{n_{B/F}(k)}{2k}\int_{k'}\frac{1\pm n_{B/F}(k')}{2k'}\int_{p'}\frac{\theta(|t|-|t|^*)}{2E'} \times(2\pi)^4\delta^{(4)}(P+K-P'-K')\left|\overline{\mathcal{M}}_{g/q}(s,t)\right|^2 q_L^2. \quad (19)$$

In the above expressions, $s=(P+K)^2$, $Q\equiv(\omega,\boldsymbol{q})\equiv P-P'$, q_T/q_L are the transverse/longitudinal components of $\boldsymbol{q}$ and $n_{B/F}$ are the Bose/Fermi distributions; the squared amplitudes are averaged over the internal degrees of freedom (colour and spin) of the incoming heavy quark and summed over the internal degrees of freedom of the initial and final state partons in the medium: N_c^2-1 colours and two transverse polarizations for a gluon, N_c colours and two helicities for a light quark. Furthermore a factor $2N_f$ is assigned to $\left|\overline{\mathcal{M}}_q\right|^2$, accounting for the identical contribution provided by all the flavours of light quarks and anti-quarks in the medium. The squared amplitudes $\left|\overline{\mathcal{M}}_{g/q}\right|^2$ defined in such a way can be obtained starting from the results given in Ref. [29] and their expressions are reported in Appendix B. The quark contribution is then obtained by squaring the corresponding amplitude in Fig. 4, given by a simple gluon exchange in the t-channel. The gluon contribution is more cumbersome and requires squaring the sum of the t, s and u-channel diagrams in Fig. 4.

2.4.3 Charm and bottom transport coefficients

In this section we display the outcome of our calculation of the heavy quark transport coefficients in the QGP and compare our results with previous findings for the same coefficients available in the literature [22,23,24,25].

As we have already mentioned, following the heavy-quark stochastic propagation in the hot environment produced in heavy ion collisions requires the knowledge of the corresponding transport coefficients for a range of temperatures from $T\sim T_c$ (where actually we expect our weak-coupling approach to underestimate their value) up to $T\sim 1$ GeV (for the case of the LHC scenarios with the highest initial energy-density).

In Fig. 5 we show our findings for $\kappa_{T/L}(p)$ for c and b quarks, at the temperature $T=400$ MeV; the coupling g has been evaluated at the scale $\mu=(3/2)\pi T$. Two important features are apparent in Fig. 5: the larger growth with the momentum p of $\kappa_L(p)$ with respect to $\kappa_T(p)$ and the very mild sensitivity to the value of the intermediate cutoff $|t|^*\sim m_D^2$. This last finding occurs in spite of the fact that, at the experimentally accessible temperatures, the coupling is not small. Such an occurrence supports the validity of the adopted approach.

A deeper insight can be gained by looking at Fig. 6, where we plot separately the soft and hard contributions to $\kappa_T(p)$ and $\kappa_L(p)$ for the case of c quarks.

We finally compare our results for the heavy-quark transport coefficients to the ones obtained using other models. We start with our previous work [22], where the HTL approximation had been applied to any value of the momentum exchange, up to a cut-off $q_{\rm max}$. Results for c and b quarks are shown in Fig. 7a and compared with the present, more realistic, treatment. The major difference one observes is in the growth of $\kappa_T(p)$ with p, which is faster in the pure HTL approach.

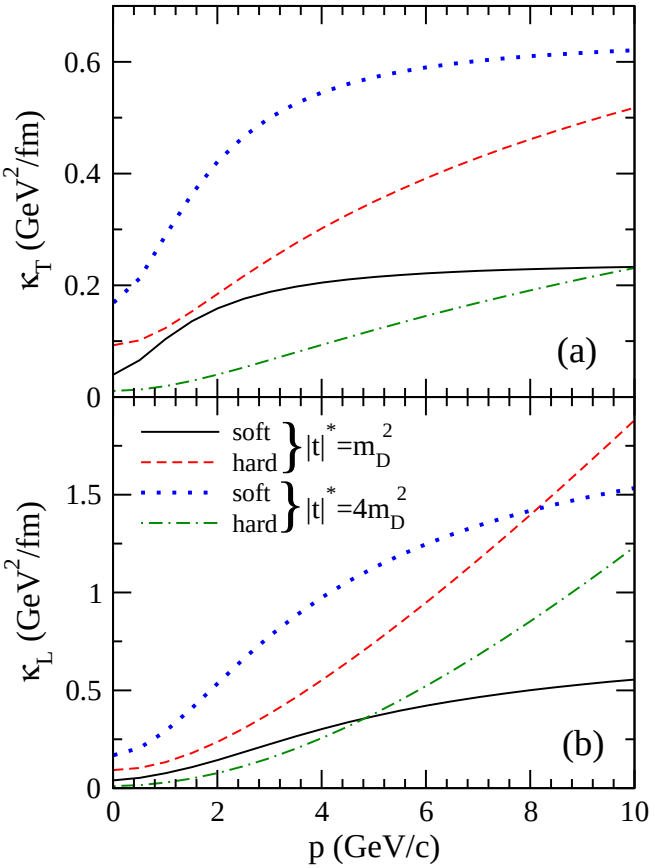

Fig. 6. The separate soft and hard contributions to $\kappa_T(p)$ (upper panel) and $\kappa_L(p)$ (lower panel) for different choices of the intermediate cutoff $|t|^*\sim m_D^2$. The curves refer to the case of a c quark, in a medium at $T=400$ MeV, with the coupling g evaluated at the scale $\mu=(3/2)\pi T$.

In Fig. 7b we summarize the outcomes of several models which can be found in the literature: the present approach (pQCD+HTL), the pure HTL result [22] and the findings of Refs. [23,24,25]. In the approach of Ref. [23], the coefficients are obtained from a kinetic pQCD calculation, with the value of $\kappa(p=0)$ tuned by hand in order to explore both strongly and weakly-coupled scenarios. In Ref. [24] the mechanism responsible for the heavy-quark thermalization is resonant scattering, with the temporary formation of finite-width D-mesons in the plasma. The authors of Ref. [25], on the other hand, resort to an effective running coupling constant and to a value of the Debye mass lower than the thermal QCD prediction. Notice how all the models based on pQCD tend to favor small-angle scattering.

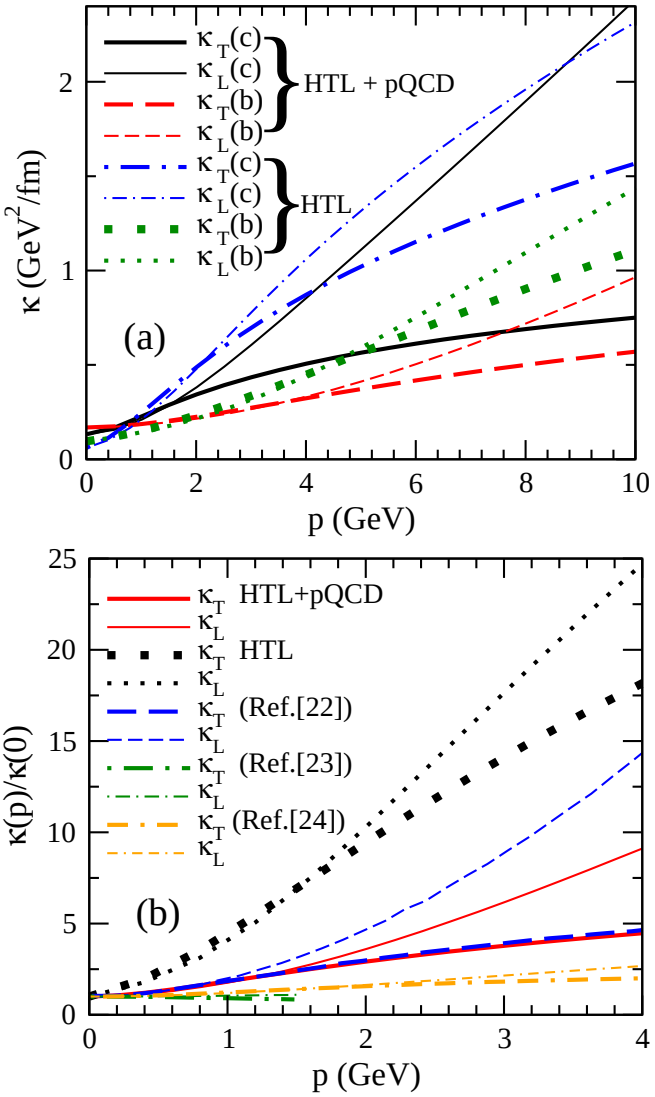

Fig. 7. (a) Transport coefficients, for both c and b quarks at $T = 400$ MeV and $\mu = (3/2)\pi T$, arising from the separate treatment of soft (HTL) and hard (pQCD) collisions (with $|t^*| = m_D^2$) compared with the pure HTL results of Ref. [22]. (b) Comparison of our results for c quarks (with $|t^*| = m_D^2$ and $\mu = (3/2)\pi T$) to the outcomes of several models [22,23,24,25] for the transport coefficients $\kappa_{T/L}(p)$ at $T = 200$ MeV.

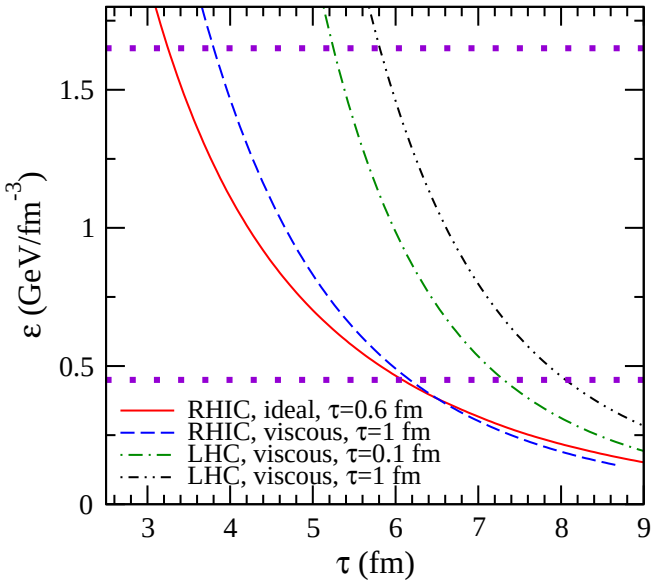

Fig. 8. Energy density in the center of the fireball at proper times around the deconfinement transition for a few hydrodynamical setups; the dotted lines correspond to $\varepsilon_{\rm QGP} = 1.65$ GeV/fm^3 and $\varepsilon_{\rm H} = 0.45$ GeV/fm^3.

2.5 Hadronization and decay

The conversion of the heavy quarks into hadrons requires two distinct steps: first, one has to decide when the quark is going to hadronize and then to apply a specific model for the transition. In the ideal hydrodynamics model of Refs. [32,33,34] a first order phase transition occurs at the temperature $T_c = 164$ MeV, lasting for a couple of fm and during which the energy density drops from $\varepsilon_{\rm QGP} = 1.65$ GeV/fm^3 to $\varepsilon_{\rm H} = 0.45$ GeV/fm^3. In the viscous hydrodynamics model of Refs. [35,36,37], on the other hand, a more realistic crossover, slightly faster because of viscosity, is employed. In Fig. 8 we display the energy density in the center of the fireball around the QGP/hadron-matter transition for a few hydrodynamical scenarios. The dotted lines mark the position of $\varepsilon_{\rm QGP}$ and $\varepsilon_{\rm H}$: we assume that hadronization is going to take place in this region of mixed phase.

Introducing the fraction of QGP in the mixed phase [26] according to

$$f_{\rm QGP} = \frac{\varepsilon - \varepsilon_{\rm H}}{\varepsilon_{\rm QGP} - \varepsilon_{\rm H}}, \qquad (20)$$

we stop the Langevin propagation of the heavy quark according to the following prescription:

- we extract the medium energy density at the heavy-quark space-time position;
- if $f_{\rm QGP}$ is larger than one, the Langevin propagation is carried on another step; otherwise
- we treat $1 - f_{\rm QGP}$ as a transition probability: given $f^i_{\rm QGP}$ — the fraction of QGP at the i-th propagation step — we draw a random number h; if $h \geq f^i_{\rm QGP}/f^{i-1}_{\rm QGP}$ then hadronization has occurred, otherwise a new Langevin step is taken and the procedure repeated at the new position.

In this way the transition from quarks to hadrons is made occur over the whole mixed phase.

2.5.1 Hadronization

Two mechanisms of hadronization should in principle be implemented, namely recombination of the heavy quark with a light quark from the medium and fragmentation. The coalescence approach has been shown to be important

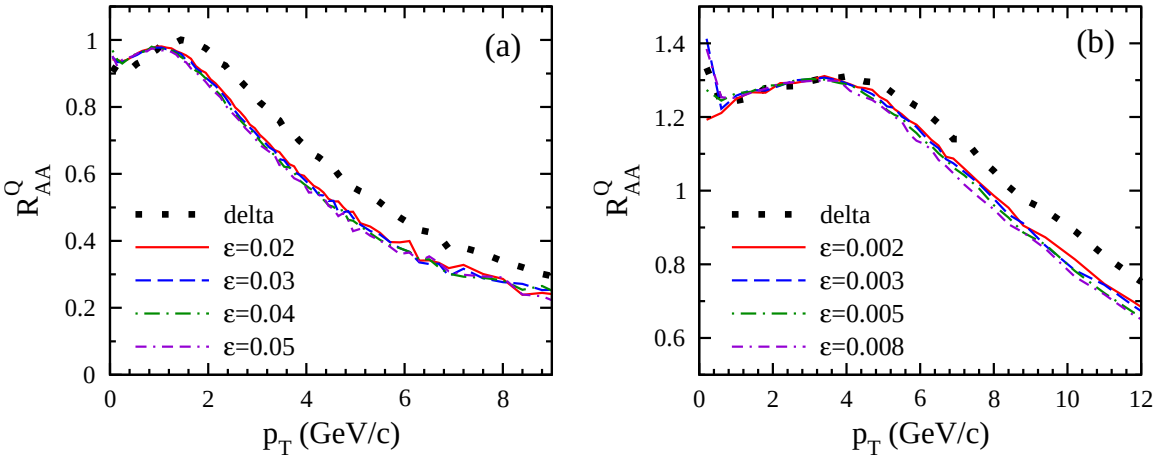

Fig. 9. Nuclear modification factor R_{AA} vs. p_T for open charm (left) and open beauty (right) hadrons for different values of the ε parameter in the Peterson fragmentation function; the dotted lines represent the delta function limit in the fragmentation function, $D(z) = \delta(1-z)$; in these examples we have used ideal hydrodynamics at RHIC for $b = 8.44$ fm and $\mu = 2\pi T$.

in the low momentum part of the spectra at RHIC [24], say for $p_T \lesssim 3$ GeV/c. In this work, we limit ourselves to let the heavy quarks hadronize by fragmentation, hence our results should be viewed as realistic for relatively large momenta, $p_T \gtrsim 3$ GeV/c at RHIC energy. Note, however, that the region where recombination is dominant might change at LHC energies.

Open charm and open beauty hadrons are produced from the charm and bottom quarks via a two-step Monte Carlo procedure. First, the resulting hadron species is assigned according to measured fragmentation ratios. In the case of charm quarks, four hadronic final states have been considered, namely D^0, D^+, D_s^+ and Λ_c^+, together with their corresponding anti-particles. The fragmentation ratios are taken from Table 4 of Ref. [55]. For bottom quarks, the considered hadronic states have been B^0, B^+, B_s^0 and Λ_b^0, together with their corresponding anti-particles. The fragmentation ratios have been taken from [56] with the only modification of assigning to the Λ_b^0 final state the probability for a bottom quark to fragment into b-baryons.

The second step is the Monte Carlo generation of the hadron momenta. This has been done starting from the momentum components (p_x, p_y and p_z) of the heavy quark out-coming from the Langevin evolution and sampling, from a Peterson fragmentation function [57], the fraction z of quark momentum that is taken by the produced hadron:

$$D(z) = \frac{k}{z} \cdot \left(1 - \frac{1}{z} - \frac{\varepsilon}{1-z}\right)^{-2}. \qquad (21)$$

The parameter k has been set in order to have the fragmentation function normalized to 1, while for ε the values 0.04 and 0.005 have been used for charm and bottom quarks, respectively. They have been chosen by comparing the fragmentation function shapes with the ones computed in Ref. [58] on a pQCD or Heavy Quark Effective Theory basis. To check the effect of the choice of the ε parameter on the resulting nuclear modification factor R_{AA} (see Eq. 23), the whole fragmentation procedure has been repeated four times varying the value of ε in the range yielding a reasonable agreement with the calculation of Ref. [58]. The obtained R_{AA} for open charm and open beauty hadrons as a function of the transverse momentum p_T for different choices of ε is shown in Fig. 9 for a specific case of $\sqrt{s}$, centrality and hydrodynamical scenario. We have checked that variations of the parameter ε by a factor two results generally in a $\lesssim 3\%$ effect on the R_{AA} of open heavy-flavoured hadrons.

2.5.2 Decays of heavy-flavour hadrons into electrons

In order to compare our calculations to the experimental data for the non-photonic single-electron ($e^{\pm}$) transverse spectra and for the corresponding nuclear modification factor R_{AA} and elliptic flow coefficient v_2, each charm or bottom hadron originated by the fragmentation of a heavy quark (as described in the previous section), is forced to decay into electrons.

This task is performed by using the decay routines implemented inside the PYTHIA event generator [59]. However, a revised table of the branching ratios for the dominant decay channels of each heavy-quark hadron has been employed, in order to replace the default values which are by now obsolete. Such table has been drawn up by taking the measured values of the branching ratios, as reported on the latest Particle Data Group review [60].

Only hadronic and semi-leptonic decay channels of charm and beauty hadrons with branching ratio $\Gamma > 10^{-4}$ have been included. Therefore the contribution of each hadron to the final electron spectra has been properly weighted by the corresponding total branching ratio.

In this way, all contributions to the electron yield (i. e., prompt electrons from $B \to e$ or $D \to e$ decays, and secondary electrons from a cascade process $B \to D \to e$) are naturally implemented in our simulation scheme, as well as the additional "background" contribution from the decay chain $B \to J/\psi \to e^+e^-$. Indeed, the latter

contribution has been subtracted from the total measured electron yields only in the most recent analyses of the PHENIX data [17].

The electron spectra originated from charm (e_c) and bottom (e_b) decays are then combined into a unique spectrum (e_{c+b}) with an appropriate weight, which accounts for the corresponding production cross section of the parent heavy quark.

3 Heavy-flavour spectra in nucleus-nucleus collisions

We have considered two kinematic regimes for high energy heavy ion collisions: Au-Au at $\sqrt{s} = 200$ GeV as in the PHENIX experiment at RHIC [16,17] and Pb-Pb at $\sqrt{s} = 5.5$ TeV, the highest energy that should be attained with AA collisions at the LHC.

In the PHENIX experiment the heavy-flavour data have been presented in several centrality classes C_1-C_2, corresponding to the fraction of the geometric cross section with impact parameter in the range $b_1 < b < b_2$:

$$f_{C_1-C2} = \frac{\int_{b_1}^{b_2} db\, b[1-\exp(\sigma_{\rm NN} T_{AB}(b)]}{\int_0^{\infty} db\, b[1-\exp(\sigma_{\rm NN} T_{AB}(b)]}, \qquad (22)$$

where $T_{AB}(b) = \int d\boldsymbol{s} T_A(\boldsymbol{s}+\boldsymbol{b}/2) T_B(\boldsymbol{s}-\boldsymbol{b}/2)$ is the nuclear overlap function and the nuclear profile function in the transverse plane $T_A(\boldsymbol{s})$ is given in Eq. (2). Our calculations are performed for a given impact parameter b, so for every centrality class we have to evaluate an average impact parameter. This can be done by equating the number of collisions in a given centrality class $< N_{\rm coll} >_{C_1-C_2} = \sigma_{\rm NN} < T_{AB} >_{C_1-C_2} = \sigma_{\rm NN} \int_{b_1}^{b_2} db\, b T_{AB}(b) / \int_{b_1}^{b_2} db\, b$ to the number of collisions at a given impact parameter $N_{\rm coll}(b) = \sigma_{\rm NN} T_{AB}(b)$ [61]. In Table 3 we show the centrality classes and the corresponding impact parameters that we have considered in the present work. At the LHC energy, lacking the experimental data, we have kept a partition similar to the one employed of RHIC.

3.1 Differential spectra

In Fig. 10 one can see the invariant yields of electrons from heavy-flavour decays in Au-Au and Pb-Pb collisions, for a specific choice of the hydrodynamical scenario (viscous hydrodynamics with $\tau_0 = 1$ fm) and of the QCD scale factor ($\mu = 3\pi T/2$). Binary-scaled pp spectra are also shown as dashed lines. We are aware that cross sections are not the best observable for studying the effect of the nuclear medium on the propagation of the heavy quarks; for this purpose the nuclear modification factor is much more suitable. It is however worth noting how the formalism is able to give a fair description of the PHENIX data over many orders of magnitude. Of course, this is also a consequence of the good performance of the pQCD outcome for the heavy quark production in NN collisions, as already discussed in Sect 2.1.

Table 3. The centrality classes and the corresponding average impact parameters at the kinematics of RHIC and LHC.

Au-Au ($\sqrt{s} = 200$ GeV)		Pb-Pb ($\sqrt{s} = 5.5$ TeV)	
C_1-C_2	b (fm)	C_1-C_2	b (fm)
0-10%	3.27	0-10%	3.45
10-20%	5.78	10-20%	6.11
20-40%	8.12	20-40%	8.58
40-60%	10.51	40-60%	11.11
60-92%	12.80	60-90%	13.45
0-92%	8.44	0-90%	8.77

3.2 Nuclear modification factor

Let us consider now the nuclear modification factor,

$$R_{AA}(p_T) = \frac{dN_{AA}/dp_T}{N_{\rm coll} dN_{pp}/dp_T}. \qquad (23)$$

In order to explore the effect and the relative importance of those ingredients of the model that are not fully under control, that is the QCD scale factor and the hydrodynamical scenario, it is instructive to start by studying the nuclear modification factor at quark level (R^Q_{AA}) first, which is the one obtained from Eq. (23) by using the spectra before hadronization (keeping the same pseudorapidity window as for the electrons). Thus, in Fig. 11 we display the charm and bottom nuclear modification factors, for the case of viscous hydrodynamics ($\tau_0 = 1$ fm) and minimum bias collisions, at both RHIC and LHC energies. Three choices for the scale factor μ are considered: the strong dependence of R_{AA} upon this parameter is quite apparent. We have not tried to fix the value of μ through a best fit to the RHIC data; however, in the following we employ the value $\mu = 3\pi T/2$, the one, among those displayed in Fig. 11, that turns out to be in better agreement at large momenta with the PHENIX data on non-photonic electrons (see below). Another important effect on R_{AA} can be appreciated by comparing the results at RHIC (panel (a)) and LHC (panel (b)) energies. Indeed, as already mentioned in Sect. 2.1, the elementary $Q\bar{Q}$ production cross sections per binary collision entering into the numerator and denominator of Eq. (23), are not the same, because of nuclear effects. R_{AA} for charm and bottom is then proportional to the ratio of the corresponding production cross sections. From Table 1 it clearly appears that for charm the relative play of shadowing and anti-shadowing is always giving rise to a quenching factor; for bottom, instead, one gets an enhancement at RHIC and a quenching at LHC (at $\sqrt{s} = 5.5$ TeV).

In Fig. 12 we display the charm and bottom nuclear modification factors for a fixed value $\mu = 3\pi T/2$ of the scale factor and several choices for the hydrodynamical scenarios (again for minimum bias collisions at RHIC and LHC). One can see that the uncertainty associated to the treatment of the hydrodynamical evolution of the QGP is quite modest compared to the one due to the heavy-quark interactions (Fig. 11). Specifically, the treatment of

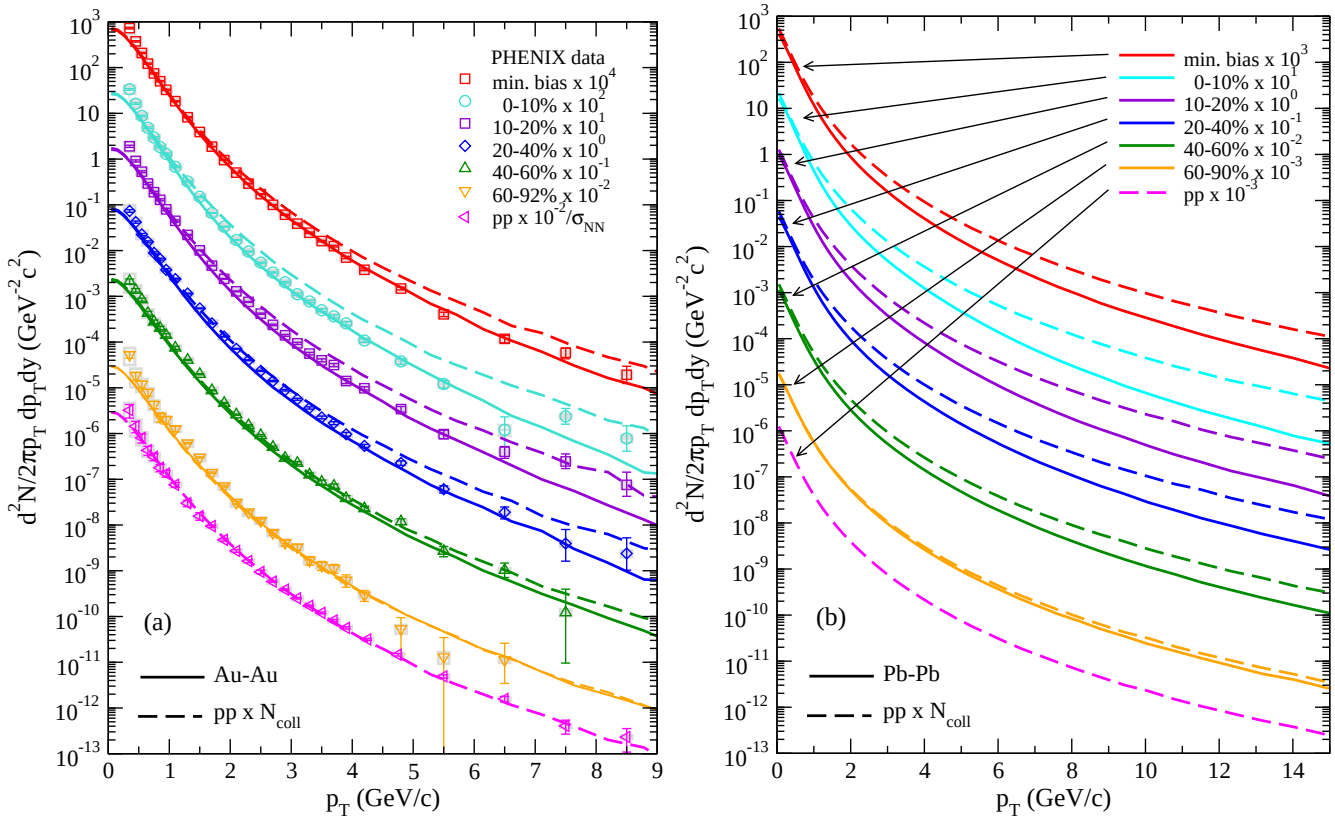

Fig. 10. (a) Invariant yields of electrons $[(e^+ + e^-)/2]$, from heavy-flavour decay in Au-Au collisions at $\sqrt{s} = 200$ GeV, at mid-rapidity as a function of transverse momentum (scaled for clarity). The experimental points represent PHENIX data [16,17]; both statistical (error bars) and systematic (gray boxes) errors are displayed. The dashed curves represent the contributions coming from electrons originating from charm and bottom quarks generated by POWHEG with inclusion of transverse broadening and rescaled by $N_{\rm coll}$. The solid curves are our results after propagation in the fireball (viscous hydrodynamics with $\tau_0 = 1$ fm, $\mu = 3\pi T/2$). (b) Invariant yields of electrons $[(e^+ + e^-)/2]$, from heavy-flavour decay in Pb-Pb collisions at $\sqrt{s} = 5.5$ TeV, at mid-rapidity as a function of transverse momentum (scaled for clarity). Dashed and solid lines as in panel (a).

the expanding fluid as either viscous or ideal has practically no influence on the heavy-quark propagation. On the other hand, some sensitivity to the choice of the starting time of the hydrodynamical evolution is seen to exist. In fact, earlier times expose the heavy quarks to higher temperatures and give rise to a more pronounced quenching of R_{AA}. At the LHC the ideal scenario with $\tau_0 = 0.1$ fm appears to be somehow in contradiction with the trend displayed by the other cases, showing smaller medium effects for a shorter equilibration time. Note that it might just signal some shortcomings of the hydrodynamical code in a regime where it has received little testing. Up to semi-peripheral collisions the effect of an earlier equilibration time is anyway moderate and smaller not only than other theoretical uncertainties, but also than the experimental ones. However, as we shall see below, for peripheral collisions the effect due to the choice of τ_0 turns out to be more important.

In Fig. 13 we display the charm and bottom nuclear modification factors of heavy quarks, open heavy-flavour hadrons and electrons for viscous hydrodynamics ($\tau_0 =$ 1 fm), scale factor $\mu = 3\pi T/2$ and minimum bias collisions at RHIC and LHC. The effect of hadronization and decay can be summed up as a general "softening" of the nuclear modification factor, especially after the decay of B mesons.

In Fig. 14 the results of our calculations of the nuclear modification factor of open heavy-flavour electrons at RHIC (for the case of viscous hydrodynamics with $\tau_0 =$ 1 fm and $\mu = 3\pi T/2$) are compared to the data from the PHENIX experiment [16,17] in all the centrality classes. Here we display the R_{AA}'s due to the electrons originating either from c-quarks or from b-quarks and their combination, showing also the statistical errors of the calculations. For $p_T \lesssim 3$ GeV/c the data are generally underestimated: this is the region where, as already mentioned, the hadronization mechanism of coalescence has been shown to be important and to give rise to an enhancement of R_{AA} [24]. At larger momenta the calculations turn out to be on the whole in agreement with the data from PHENIX, with an evident contribution from the bottom quarks.

The above considerations are valid in all the centrality classes, except perhaps the most peripheral one (60-92%): here the effect of the medium is expected to be pretty weak and, indeed, our calculation does not show, at low

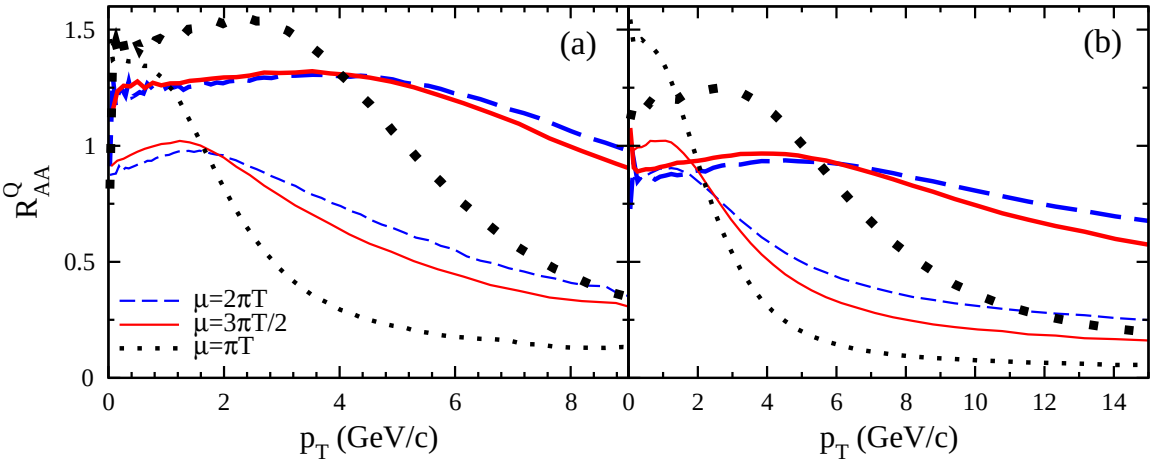

Fig. 11. (a) The heavy-quark nuclear modification factor at RHIC for viscous hydrodynamics ($\tau_0 = 1$ fm), $b = 8.44$ fm and different choices of the QCD scale factor; both c (light lines) and b (heavy lines) quarks are shown. (b) As in panel (a), but for LHC at $b = 8.77$ fm.

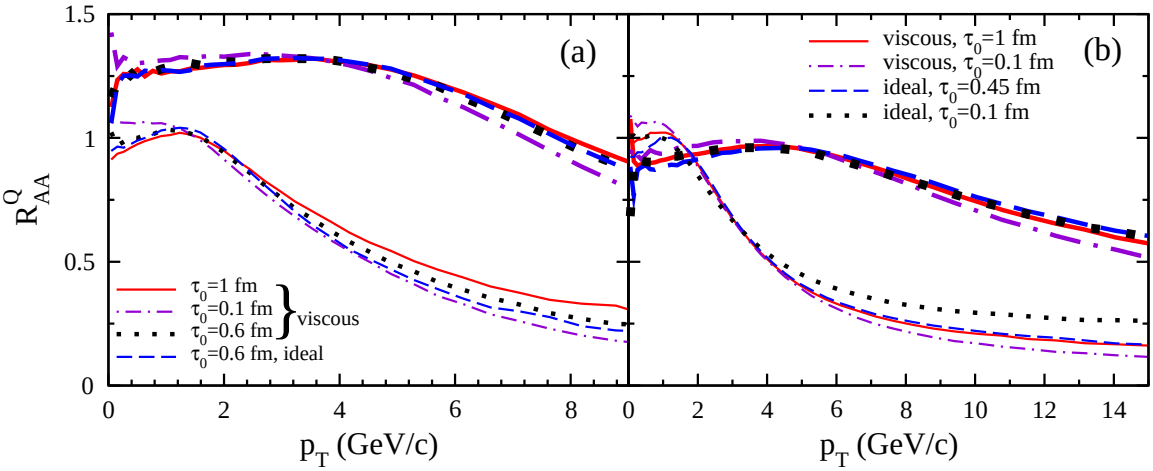

Fig. 12. (a) The heavy-quark nuclear modification factor at RHIC for $\mu = 3\pi T/2$, $b = 8.44$ fm and different hydrodynamical scenarios; both c (light lines) and b (heavy lines) quarks are shown. (b) As in panel (a), but for LHC at $b = 8.77$ fm.

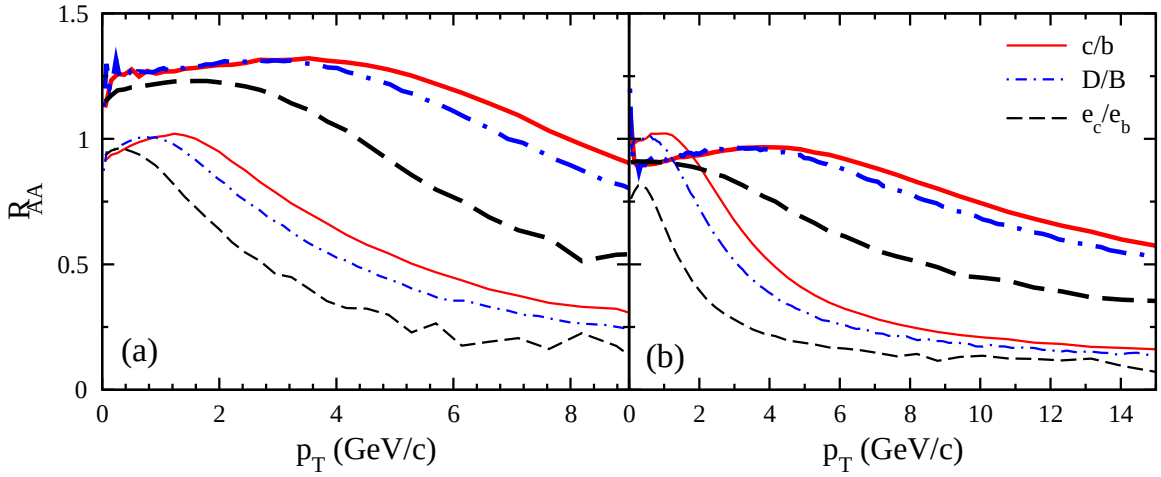

Fig. 13. (a) The nuclear modification factor of heavy quarks, open heavy-flavour hadrons and electrons at RHIC for $\mu = 3\pi T/2$, viscous hydrodynamics ($\tau_0 = 1$ fm) and $b = 8.44$ fm; both the charm (light lines) and bottom (heavy lines) sectors are shown. (b) As in panel (a), but for LHC at $b = 8.77$ fm.

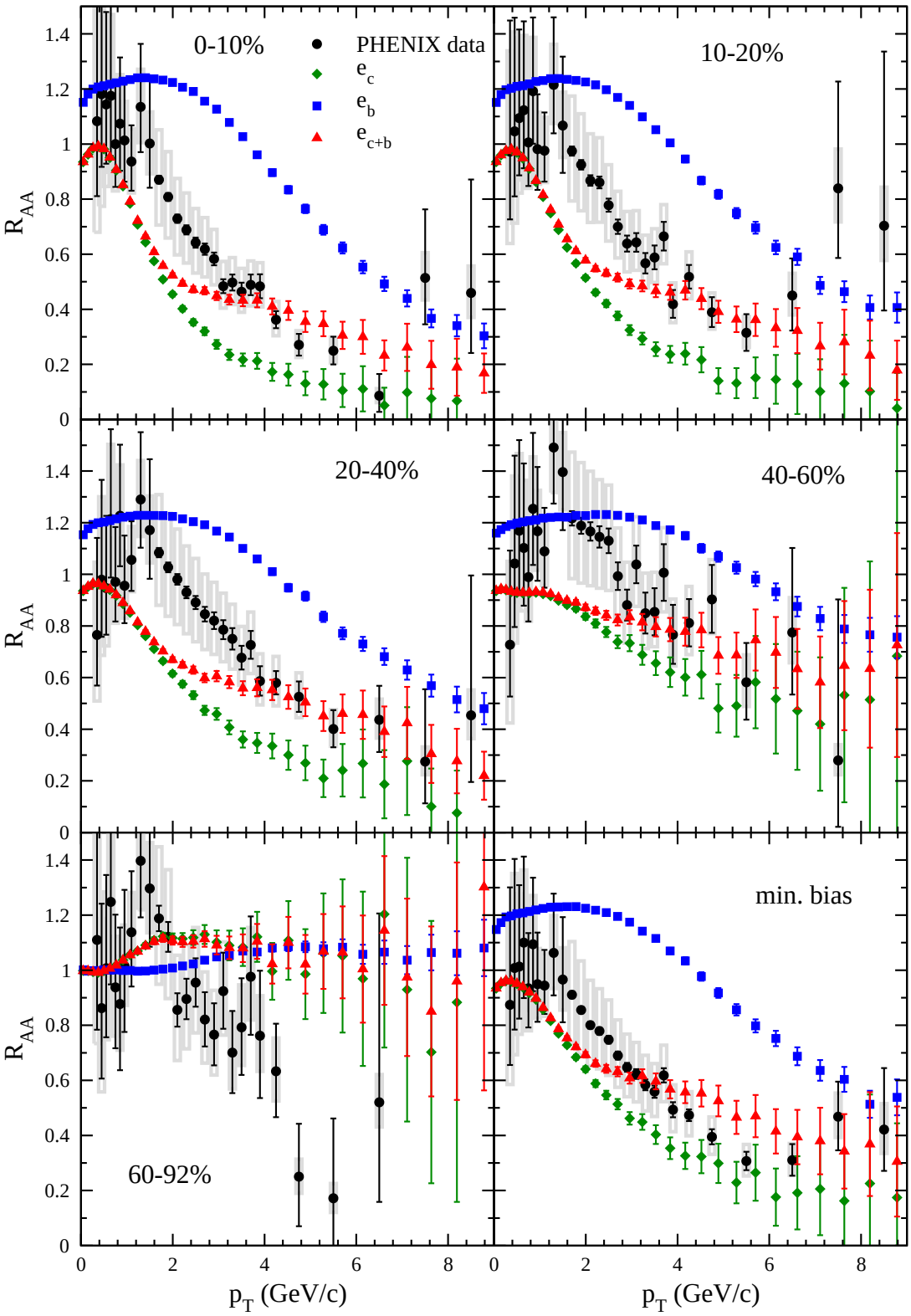

Fig. 14. The nuclear modification factor of open heavy-flavour electrons at RHIC for $\mu = 3\pi T/2$ and viscous hydrodynamics ($\tau_0 = 1$ fm) in various centrality classes. The circles are data from the PHENIX experiment [16,17], including both statistical (error bars) and systematic (grey boxes) errors; the other points (with the statistical errors shown) are the outcome of our calculations for electrons originating from charm and bottom quarks and their combination.

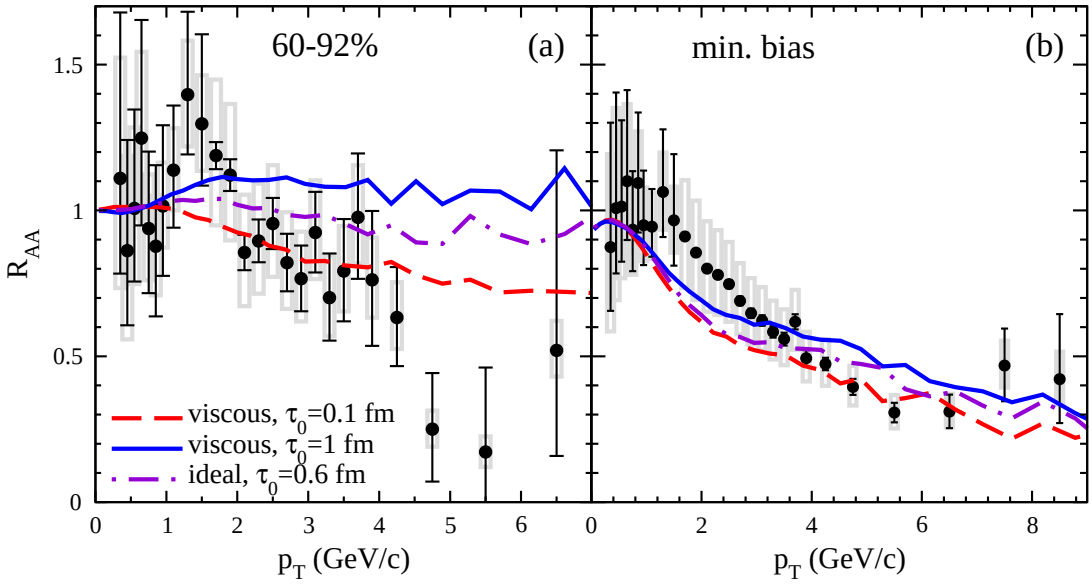

Fig. 15. (a) The nuclear modification factor of open heavy-flavour electrons from peripheral collisions at RHIC for $\mu = 3\pi T/2$ and different starting times for the hydrodynamical evolution. Data are from the PHENIX experiment [16,17]. The theoretical curves show (without statistical errors) the total yield of electrons from charm and bottom quarks. (b) As in panel (a), but for minimum bias collisions.

momenta, any underestimation of the data, but rather it overshoots them at intermediate momenta. In Fig. 15(a) we compare the PHENIX data for the most peripheral centrality class to the outcome of calculations based on different initial times. A reduction of τ_0 from 1 fm to 0.1 fm in all the other centrality classes gives rise to a rather mild effect, well within the theoretical and experimental uncertainties, as one can see, e. g., in Fig. 15(b) for minimum bias collisions. For very peripheral collisions, on the other hand, the highest temperatures associated to earlier equilibration times provides a stronger signature. Note, however, that for this centrality class — where one is moving from a region where the core of the nuclear density distributions is probed to a region where only the tails of the density distributions are involved — the approximation based on the use of an average impact parameter might be less reliable.

In Fig. 16 we display the nuclear modification factor of open heavy-flavour electrons at LHC@5.5 TeV for QCD scale factor $\mu = 3\pi T/2$ and two choices of the equilibration time. The features of R_{AA} appear to be quite similar to the case of RHIC, except for a larger quenching at small momenta — due in our calculation to the smaller pp over AA ratio of the $c\bar{c}$ production cross sections — and for a slightly smaller value at large momenta. The choice of the equilibration time, as already discussed, has a mild effect, except perhaps on the most peripheral collisions.

In Fig. 17 the nuclear modification factor of open heavy-flavour electrons, obtained by integrating the electron yields above a given transverse momentum, is reported as a function of the number of participants. When the integration range covers most of the spectrum, one should get the ratio of the total electron yields in AA and pp collisions, that is, in practice, the ratio of the respective heavy-quark production cross sections. When only large transverse momenta are selected, one observes the quenching of R_{AA} due to the softening of the heavy-quark spectra by the medium. The calculations are again in fair agreement with the PHENIX data, except, as already noted, for the most peripheral collisions. These, however, represent a real puzzle, since they seem to imply that the strongest medium effects manifest themselves with the highest and the lowest numbers of participants.

Finally, in this study we have also tried to understand the amount of uncertainty introduced by an approximation that is, to our knowledge, always employed in this kind of calculations, i. e. the use of an average impact parameter to represent a given centrality class. In Fig. 18 the minimum bias nuclear modification factor of open heavy-flavour electrons at RHIC and LHC is displayed, comparing the results obtained by using a single average impact parameter to those obtained by combining the weighted spectra in all the centrality (sub)classes (0-10%, 10-20%, ...). The effect is not dramatic compared to other uncertainties, especially at LHC, but for an accurate estimate of R_{AA} it will have to be accounted for.

3.3 Elliptic flow coefficient

The anisotropy parameter associated to the elliptic flow of the heavy quark is defined as

$$v_2(p_T) = \frac{\int d\phi \frac{d^2N_{AA}}{d\phi dp_T} \cos 2\phi}{\int d\phi \frac{d^2N_{AA}}{d\phi dp_T}}, \qquad (24)$$

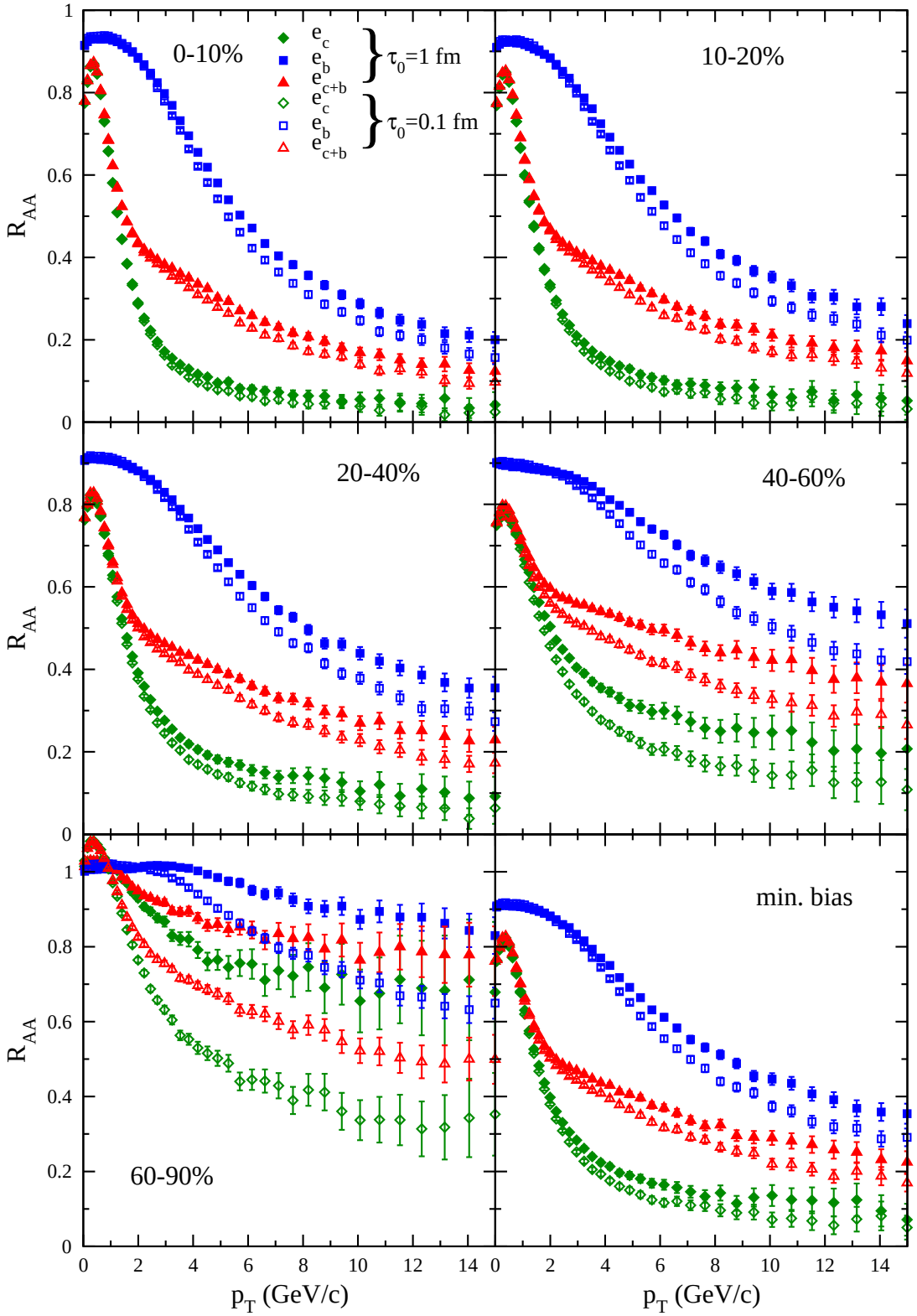

Fig. 16. The nuclear modification factor of open heavy-flavour electrons at LHC@5.5 TeV for $\mu = 3\pi T/2$ and viscous hydrodynamics ($\tau_0 = 1$ fm and 0.1 fm) in various centrality classes. Electrons originating from charm and bottom quarks and their combination are shown, including the statistical errors.

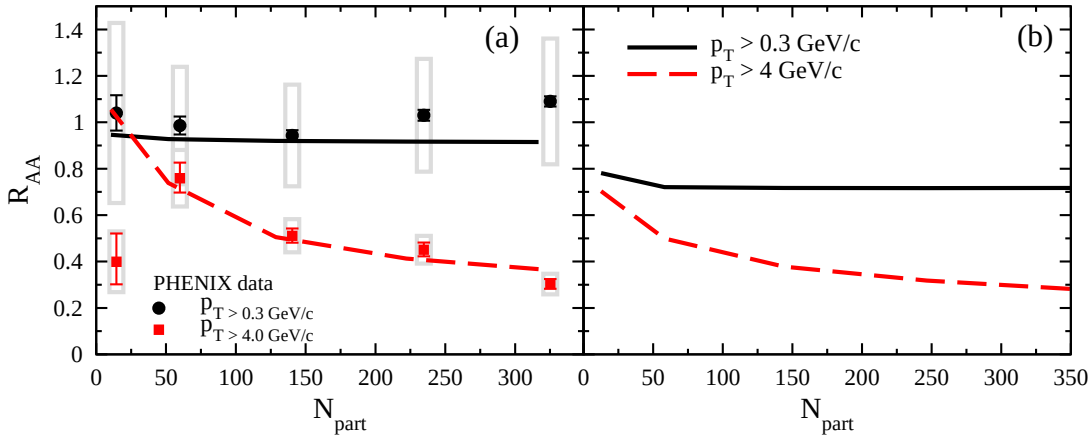

Fig. 17. The nuclear modification factor of open heavy-flavour electrons at RHIC (a) and LHC@5.5 TeV (b) for $\mu = 3\pi T/2$ and viscous hydrodynamics ($\tau_0 = 1$ fm), obtained by integrating the electron yields over the indicated momentum ranges, as a function of the number of participants. The data points from the PHENIX experiment [17], including both statistical (error bars) and systematic (grey boxes) errors.

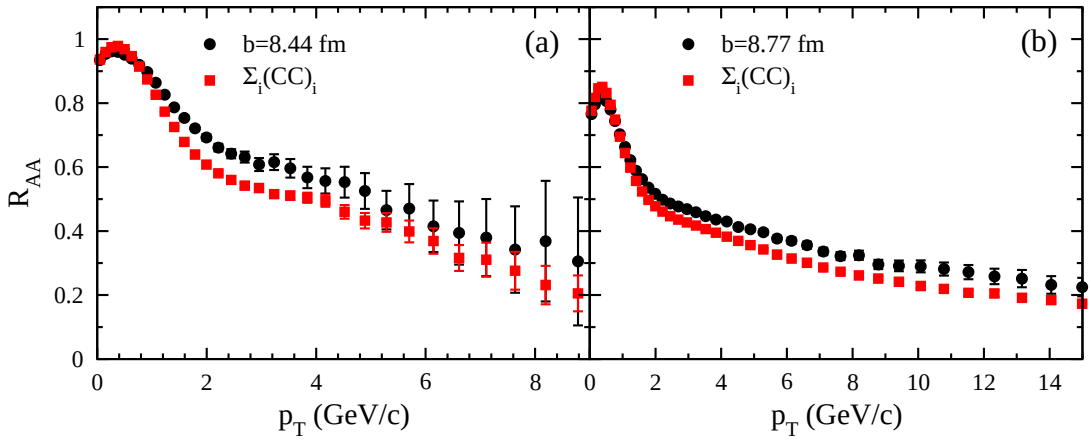

Fig. 18. The nuclear modification factor of open heavy-flavour electrons at RHIC (a) and LHC@5.5 TeV (b) for $\mu = 3\pi T/2$ and viscous hydrodynamics ($\tau_0 = 1$ fm). The circles refer to the calculation at a fixed average impact parameter, the squares to the weighted sum of the results in all the centrality classes.

where $d^2N_{AA}/d\phi dp_T$ is the doubly differential yield of open heavy-flavour electrons, of D and B mesons or of c and b quarks, depending on which observable one is considering.

In Fig. 19 we display the charm and bottom elliptic flow coefficients of heavy quarks, open heavy-flavour hadrons and electrons for viscous hydrodynamics ($\tau_0 = 1$ fm), scale factor $\mu = 3\pi T/2$ and minimum bias collisions at RHIC and LHC. In a momentum range up to a few GeV/c the heavy quark v_2 is represented by a growing function of p_T. Since, as already noted, hadronization and decay to electrons produce a softening of the respective spectra, the net result is a stronger anisotropy of B/D mesons with respect to c/b quarks and an even stronger one for the open heavy-flavour electrons. At the LHC energy one gets larger elliptic flow coefficients, especially the bottom contribution.

In Fig. 20 we display the total v_2 of open heavy-flavour electrons for minimum bias events at RHIC and LHC. The calculation at RHIC energy is compared to the data from PHENIX, which, however, are available only up to $p_T \approx 4$ GeV/c. Our results for $\tau_0 = 1$ fm underestimate the data for $p_T < 3$ GeV/c, as they also do in the case of the nuclear modification factor. The already mentioned coalescence mechanism for the hadronization process is known to be important in this momentum region and to provide an enhancement of both R_{AA} and v_2 [24]. Note, however, that an earlier equilibration time gives rise to an anisotropy parameter closer to the data. At the LHC energy, one observes a stronger anisotropy for the exclusive c and b contributions, while the effect due to the choice of τ_0 turns out to be milder.

4 Summary and conclusions

In this work we intended to provide a consistent study of the stochastic dynamics of heavy quarks (c and b) in the hot environment formed in high-energy heavy-ion collision experiments. The background medium has been taken as

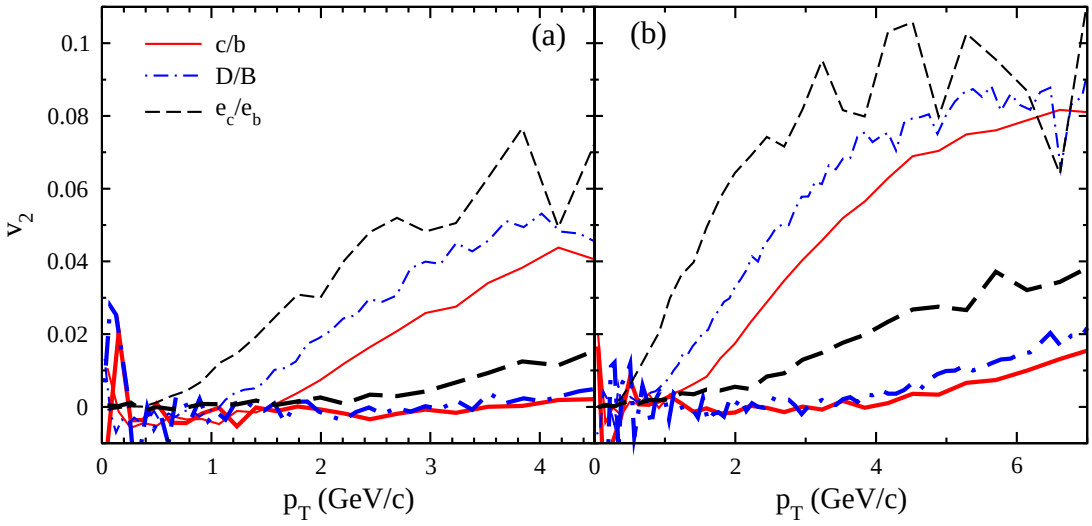

Fig. 19. (a) The minimum bias anisotropy parameter v_2 of heavy quarks, open heavy-flavour hadrons and electrons at RHIC for $\mu = 3\pi T/2$, viscous hydrodynamics ($\tau_0 = 1$ fm) and $b = 8.44$ fm; both the charm (light lines) and bottom (heavy lines) sectors are shown. (b) As in panel (a), but for LHC at $b = 8.77$ fm.

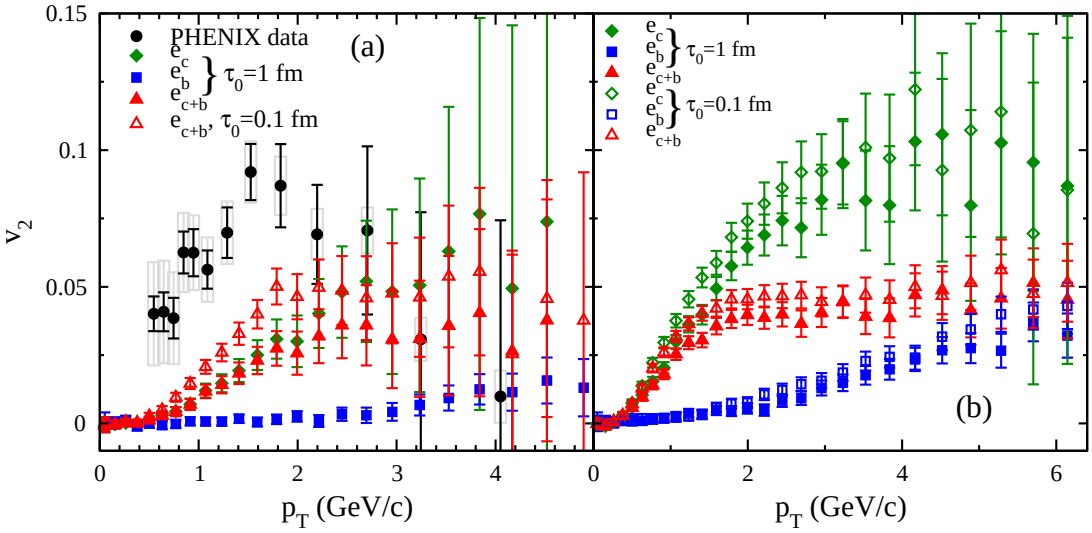

Fig. 20. (a) The minimum bias anisotropy parameter v_2 for open heavy-flavour electrons at RHIC for $\mu = 3\pi T/2$ and viscous hydrodynamics ($\tau_0 = 1$ fm and 0.1 fm). The circles are data from the PHENIX experiment [16,17], including both statistical (error bars) and systematic (grey boxes) errors; the other points (with the statistical errors shown) are the outcome of our calculations for electrons originating from charm and bottom quarks and their combination. (b) As in panel (a), but for LHC and two choices of τ_0.

a fluid (the QGP locally in thermal equilibrium), whose evolution is governed by relativistic hydrodynamics, while the interaction of the heavy quarks with the plasma has been treated within a weakly-coupled framework.

To accomplish this programme one has to evaluate the relevant transport coefficients (accounting, in our case, for the squared momentum acquired per unit time) characterizing the dynamics of the heavy quarks coupled to the medium. We have done this by summing the contributions of soft and hard collisions in the plasma. The first ones have been described in the HTL approximation, while the latter have been treated within a kinetic pQCD calculation. The propagation of the heavy quarks in the expanding plasma has been described by a relativistic generalization of the Langevin equation.

When the hydrodynamical evolution of the QGP has reached the region of energy density where the quark to hadron transition may occur, the heavy quarks are let hadronize and eventually decay into electrons: in fact, their spectra at RHIC are so far the only source of information on the heavy-flavour dynamics in the QGP (while waiting for the forthcoming open-charm analyses at RHIC

and LHC). Results have been presented for the invariant single-electron spectra, for the nuclear modification factor R_{AA} and for the elliptic flow coefficient v_2.

The main goal of our work has been first of all to provide of a fully consistent weakly-coupled calculation (accounting for medium effects at the lowest non-trivial order), to be viewed as a benchmark for more advanced studies or less conventional scenarios. Nevertheless, the overall degree of agreement with the current experimental data looks quite satisfactory, suggesting that the actual values of the heavy-quark transport coefficients might be not too different from what predicted by a weak coupling approach. In particular, for large enough values of p_T (say $p_T \gtrsim 3$ GeV/c), it has been possible to reproduce the experimental quenching of the single-electron spectra for any centrality class (except perhaps the most peripheral events, which will be discussed in more detail in the following). On the other hand, at low p_T ($\lesssim 3$ GeV/c) our results for R_{AA} are consistently below the data, predicting too much quenching. This outcome might be a consequence of the implemented hadronization scheme, where we have accounted only for the fragmentation mechanism (which entails a degradation of the heavy-quark momentum). Hadronization through coalescence with light partons of the medium could help in getting closer to the experimental data. Hadronization represents therefore an important source of systematic uncertainty for moderate values of p_T.

Concerning the sensitivity to the properties of the background medium, in general we have found a rather mild dependence on the hydrodynamical scenario (ideal or viscous, with different choices of τ_0) used to describe the plasma, except for the most peripheral events, which deserve some separate comments. Quite surprisingly, though with large error bars, experimental data on heavy-flavour electrons from RHIC display a sizable quenching of the p_T-spectra even in the $60-92\%$ centrality class. As shown in Sect. 3.2, employing a value of $\tau_0 \sim 1$ fm, as often done in hydrodynamical simulations at RHIC energy, would lead to $R_{AA} \sim 1$, thus essentially showing the absence of medium effects. On the other hand, assuming a much faster thermalization, by setting $\tau_0 = 0.1$ fm, it is possible to get much closer to the data. Notice that with such a small value for the equilibration time it is also possible to reach a slightly more satisfactory agreement with the elliptic flow v_2 measured for heavy-flavour electrons at RHIC. At the present stage we cannot draw any definite conclusion on this point and we leave it as an open issue for future investigation.

Besides analyzing the RHIC data, we have also provided predictions for LHC (at the highest energy that should be reached, $\sqrt{s}_{NN} = 5.5$ TeV). In the absence of experimental data to constrain the properties of the background medium, we have explored some of the possible hydrodynamical scenarios proposed in the literature. As a general outcome, charm is found to display a stronger quenching and a much larger elliptic flow with respect to RHIC. Also the spectra of bottom are more suppressed and characterized by a modest elliptic flow. However, in the combined electron spectra (e_{c+b}), due to the larger relative weight of the b contribution, differences between RHIC and LHC are less evident. The possibility by the ongoing experiments of identifying the separate contribution of charm, by looking at its hadronic decay channels, will certainly increase the amount of information on the heavy-flavour dynamics provided by the data. Heavy-ion collisions at LHC are presently being performed at the NN center-of-mass energy $\sqrt{s}_{NN} = 2.76$ TeV: work is in progress in order to analyze, within the framework presented in this article, also this kinematical setup.

We thank R. Averbeck, G. Ridolfi, A. Toia and J. Bielcik for helpful discussions and P.B. Gossiaux for providing us his data on the transport coefficients.

A Transverse momentum broadening of heavy quarks in nucleus-nucleus collisions

As explained in the text, our procedure to account for the transverse momentum broadening in a collinear collision consists in adding, to the heavy quarks generated in each event, a transverse component randomly chosen according to a Gaussian distribution [41]

$$g(k_T) = \frac{1}{\pi \langle k_T^2 \rangle} \exp(-k_T^2/\langle k_T^2 \rangle). \tag{25}$$

As already mentioned, for pp collision the typical value of $\langle k_T^2 \rangle_{\rm NN}$ is 1 GeV^2/c^2.

Let us now consider a collision between the nuclei A and B at impact parameter $\boldsymbol{b}$, in which a $Q\bar{Q}$ pair is produced in a hard event occurring at position $\boldsymbol{s}$ in the transverse plane (measured with respect to the center of nucleus A) and at the longitudinal coordinates (measured in the rest frames of the respective nuclei) z_A and z_B. The heavy-quark pair will be produced by partons (mainly gluons) that have already crossed a certain thickness of nuclear matter, thus having acquired some transverse momentum. In Refs. [44,45] the average squared-momentum of the produced $Q\bar{Q}$ heavy meson has been found to be given, neglecting absorption effects, by the expression

$$\begin{aligned} \langle p_T^2 \rangle_{AB}^{Q\bar{Q}}(\boldsymbol{b}, \boldsymbol{s}, z_A, z_B) = \langle p_T^2 \rangle_{\rm NN}^{Q\bar{Q}} \\ + a_{gN}[l_A(\boldsymbol{s}, z_A) + l_B(\boldsymbol{s}-\boldsymbol{b}, z_B)], \end{aligned} \tag{26}$$

where $\langle p_T^2 \rangle_{\rm NN}^{Q\bar{Q}}$ is the value for the same quantity in NN collisions and

$$\begin{aligned} l_A(\boldsymbol{s}, z_A) &\equiv \int_{-\infty}^{z_A} dz\, \rho_A(\boldsymbol{s}, z)/\rho_0 \\ l_B(\boldsymbol{s}-\boldsymbol{b}, z_b) &\equiv \int_{z_B}^{+\infty} dz\, \rho_B(\boldsymbol{s}-\boldsymbol{b}, z)/\rho_0 \end{aligned} \tag{27}$$

represent the lengths traveled by a gluon of B in nucleus A and vice versa. In Eq. (27) $\rho(\boldsymbol{s}, z)$ is the nuclear density function and ρ_0 is the central nuclear density. The parameter a_{gN} represents the average squared (transverse)

momentum per unit length acquired by a gluon in nuclear matter. At the energy of SPS one finds good agreement with the J/ψ data for $a_{gN} \approx 0.08$ GeV^2/fm [46].

Let us now apply the above scheme, developed for charmonia, to the problem of inclusive single-particle spectra. The random transverse momentum kick of the pair reflects the one acquired by the incoming gluons in crossing nuclear matter. It is shared by the two quarks,

$$\boldsymbol{k}_T^{Q\bar{Q}} = \boldsymbol{k}_T^{Q} + \boldsymbol{k}_T^{\bar{Q}}, \tag{28}$$

and for a random choice of the azimuthal angle of each quark of the pair one has:

$$\langle \boldsymbol{k}_T^2 \rangle^{Q\bar{Q}} = \langle \boldsymbol{k}_T^2 \rangle^{Q} + \langle \boldsymbol{k}_T^2 \rangle^{\bar{Q}} + 2\langle k_T^Q k_T^{\bar{Q}} \cos\phi_{Q\bar{Q}} \rangle \equiv 2\langle \boldsymbol{k}_T^2 \rangle^{Q}. \tag{29}$$

In general one does not know the longitudinal coordinate of the hard event, so that one takes an average over the longitudinal positions z_A and z_B, with a weight given by the corresponding local nuclear density. The average squared momentum used in the distribution of Eq. (25) to extract the transverse momentum kick for the heavy quarks is then:

$$\begin{aligned}\langle k_T^2 \rangle_{AB}^{Q}(\boldsymbol{b},\boldsymbol{s}) &= \langle k_T^2 \rangle_{\rm NN}^{Q} \\ &+ \frac{a_{gN}}{2}\left[\frac{\int_{-\infty}^{+\infty} dz_A\, \rho_A(\boldsymbol{s},z_A) l_A(\boldsymbol{s},z_A)}{\int_{-\infty}^{+\infty} dz_A\, \rho_A(\boldsymbol{s},z_A)} + \right. \\ &\left. + \frac{\int_{-\infty}^{+\infty} dz_B\, \rho_B(\boldsymbol{s}-\boldsymbol{b},z_B) l_B(\boldsymbol{s}-\boldsymbol{b},z_B)}{\int_{-\infty}^{+\infty} dz_B\, \rho_B(\boldsymbol{s}-\boldsymbol{b},z_B)} \right]. \end{aligned} \tag{30}$$

Note that we keep track of the transverse position of the hard event, since the transverse momentum kick is imparted to heavy quarks distributed in the transverse plane according to binary-collision scaling.

The parameter a_{gN} has been fixed in Refs. [44,45] at an energy lower that the ones we are interested in ($\sqrt{s} =$ 158 GeV [46]). In order to extrapolate its value to the RHIC and LHC regimes we have considered the transverse squared momentum of Eq. (30) averaged over the $Q\bar{Q}$ pair transverse position $\boldsymbol{s}$ and over the impact parameter $\boldsymbol{b}$. This same quantity has been modeled in Ref. [62,41] in terms of the squared-momentum transfer per collision,

$$\Delta^2(\mu) = 0.225 \frac{\ln^2(\mu/\text{GeV})}{1+\ln(\mu/\text{GeV})}\,\text{GeV}^2, \tag{31}$$

($\mu \cong 2m_Q$ being the interaction scale) and of the inelastic nucleon-nucleon cross section $\sigma_{\rm NN}$. A straightforward comparison of our expression with the one of Ref. [41] yields, indeed,

$$a_{gN} = \Delta^2 \sigma_{\rm NN} \rho_0, \tag{32}$$

$\sigma_{\rm NN}$ being the total inelastic NN cross section and ρ_0 the central nuclear density, and leads to the values displayed in Table 4.

Table 4. The total nucleon-nucleon inelastic cross section and the parameter $a_{gN}^{Q\bar{Q}}$ at different kinematics.

$\sqrt{s}$ (GeV)	158	200	5500
$\sigma_{\rm NN}$ (mb)	33	42	72
$a_{gN}^{c\bar{c}}$ (GeV^2/fm)	0.081	0.10	0.17
$a_{gN}^{b\bar{b}}$ (GeV^2/fm)	0.221	0.27	0.47

B Momentum diffusion coefficients: calculation of the hard contribution

In this Appendix we provide some details on the calculation of the hard-collision contribution to the momentum-diffusion coefficients. The squared amplitude for scattering on quarks (Fig. 4) reads:

$$\begin{aligned}\left|\overline{\mathcal{M}}_q(s,t)\right|^2 &= 2N_f 2N_c \alpha_s^2 \pi^2 \frac{64}{9} \\ &\times \frac{(M^2-u)^2 + (s-M^2)^2 + 2M^2 t}{t^2},\end{aligned} \tag{33}$$

where, as mentioned in the text, the factor $2N_f$ arises from the equal contribution of all light quark and antiquark flavours, while the further factor $2N_c$ with respect to Ref. [29] reflects our summing, rather than averaging, over the helicities and colours of the incoming light quark. For scattering on gluons (Fig. 4) one gets

$$\begin{aligned}\left|\overline{\mathcal{M}}_g(s,t)\right|^2 &= 2(N_c^2-1)\alpha_s^2\pi^2 \\ &\times \left[32\frac{(s-M^2)(M^2-u)}{t^2} \right. \\ &+ \frac{64}{9}\frac{(s-M^2)(M^2-u)+2M^2(s+M^2)}{(s-M^2)^2} \\ &+ \frac{64}{9}\frac{(s-M^2)(M^2-u)+2M^2(M^2+u)}{(M^2-u)^2} \\ &+ \frac{16}{9}\frac{M^2(4M^2-t)}{(s-M^2)(M^2-u)} \\ &+ 16\frac{(s-M^2)(M^2-u)+M^2(s-u)}{t(s-M^2)} \\ &\left. - 16\frac{(s-M^2)(M^2-u)-M^2(s-u)}{t(M^2-u)} \right],\end{aligned} \tag{34}$$

where the factor $2(N_c^2-1)$ with respect to Ref. [29] stems from summing over the polarization and the colours of the incoming gluon.

In order to perform the phase space integration in Eqs. (18) and (19), it is convenient to express the longitudinal and transverse squared momenta exchanged in the collision in terms of the energy ω lost by the heavy quark and of the Mandelstam variable t. One has

$$q_L^2 = \frac{(2E\omega+|t|)^2}{4p^2} \quad \text{and} \quad q_T^2 = \omega^2 + |t| - \frac{(2E\omega+|t|)^2}{4p^2}, \tag{35}$$

so that one can follow the procedure of Ref. [19] for the evaluation of integrals like ($\int_k \equiv \int d\boldsymbol{k}/(2\pi)^3$)

$$I[f] = \frac{1}{2E}\int_k \frac{n_{B/F}(k)}{2k}\int_{k'}\frac{1\pm n_{B/F}(k')}{2k'}\int_{p'}\frac{\theta(|t|-|t|^*)}{2E'} \times(2\pi)^4\delta^{(4)}(P+K-P'-K')f(s,t,\omega). \quad (36)$$

One gets

$$I[f] = \frac{1}{16\pi^2 pE}\int_k \frac{n_{B/F}(k)}{2k}\int_{|t|^*}^{|t|^{\max}} d|t|\int_{\omega_{\min}}^{\omega_{\max}}\frac{d\omega}{\sqrt{g(\omega)}} \times[1\pm n_{B/F}(k+\omega)]f(s,t,\omega), \quad (37)$$

where

$$g(\omega) = -a^2\omega^2 + b\omega + c, \quad (38)$$

being

$$a = \frac{s-M^2}{p}, \quad b = \frac{2|t|}{p^2}\left[E(s-M^2)-k(s+M^2)\right], \quad (39)$$

$$c = \frac{|t|}{p^2}\left[4p^2k^2-(s-M^2-2Ek)-|t|((E+k)^2-s)\right]$$

and

$$\omega_{\max/\min} = \frac{b\pm\sqrt{b^2+4a^2c}}{2a^2}. \quad (40)$$

From $b^2+4a^2c\geq 0$ one gets then:

$$|t|^{\max} = \frac{(s-M^2)^2}{s}. \quad (41)$$

Hard collisions provide a non-vanishing contribution only as long as $|t|^{\max} > |t|^*$. This allows to set the relevant range of integration over $\boldsymbol{k}$, which is given by:

$$k > \frac{|t|^*}{4E(1+v)}\left(1+\sqrt{1+\frac{4M^2}{|t|^*}}\right), \quad (42)$$

$$-1 < \cos\theta_{kp} < \min\left[1, \frac{1}{v}-\frac{|t|^*}{4Ekv}\left(1+\sqrt{1+\frac{4M^2}{|t|^*}}\right)\right].$$

References

1. S.S. Adler et al. (PHENIX collaboration), Phys. Rev. Lett. **91**, 072301 (2003)
2. J. Adams et al. (STAR collaboration), Phys. Rev. Lett. **91**, 172302 (2003)
3. S.S. Adler et al. (PHENIX collaboration), Phys. Rev. Lett. **91**, 182301 (2003)
4. J. Adams et al. (STAR collaboration), Phys. Rev. Lett. **92**, 052302 (2004)
5. K. Aamodt et al. (ALICE collaboration), arXiv:1011.3914 [nucl-ex]
6. K. Aamodt et al. (ALICE collaboration), arXiv:1012.1004 [nucl-ex]
7. M. Gyulassy, P. Levai, I. Vitev, Phys. Rev. Lett. **26**, 5535 (2000)
8. R. Baier, Y.L. Dokshitzer, A.H. Mueller, S. Peigne, D. Schiff, Nucl. Phys. B **484**, 265 (1997)
9. C. Salgado, U.A. Wiedemann, Phys. Rev. D **68**, 014008 (2003)
10. P.B. Arnold, G.D. Moore, L.G. Yaffe, J. High Energy Phys. **0206**, 030 (2002)
11. L.D. Landau, I.J. Pomeranchuk, Dokl. Akad. Nauk. SSSR **92**, 535 (1953); **92**, 735 (1953)
12. A.B. Migdal, Phys. Rev. **103**, 1811 (1956)
13. Y.L. Dokshitzer, D.E. Kharzeev, Phys. Lett. B **519**, 199 (2001)
14. N. Armesto, A. Dainese, C.A. Salgado, U.A. Wiedemann, Phys. Rev. D **71**, 054027 (2005)
15. N. Armesto, C.A. Salgado, U.A. Wiedemann, Phys. Rev. D **69**, 114003 (2004)
16. A. Adare et al. (PHENIX Collaboration), Phys. Rev. Lett. **98**, 172301 (2007)
17. A. Adare et al. (PHENIX Collaboration), arXiv:1005.1627 [nucl-ex].
18. E. Braaten, M.H. Thoma, Phys. Rev. D **44**, 1298 (1991); **44**, R2625 (1991)
19. S. Peigné, A. Peshier, Phys. Rev. D **77**, 014015 (2008)
20. S. Peigné, A. Peshier, Phys. Rev. D **77**, 114017 (2008)
21. B. Svetitsky, Phys. Rev. D **37**, 2484 (1988)
22. A. Beraudo, A. De Pace, W.M. Alberico, A. Molinari, Nucl. Phys. A **831**, 59 (2009)
23. G.D. Moore, D. Teaney, Phys. Rev. C **71**, 064904 (2005)
24. H. van Hees, V. Greco and R. Rapp, Phys. Rev. C **73**, 034913 (2006)
25. P.B. Gossiaux, J. Aichelin, Phys. Rev. C **78**, 014904 (2008)
26. Y. Akamatsu, T. Hatsuda, T. Hirano, Phys. Rev. C **79**, 054907 (2009)
27. S.K. Das, Jan-e Alam, P. Mohanty, Phys. Rev. C **80**, 054916 (2009)
28. P.B. Gossiaux, R. Bierkandt, J. Aichelin, Phys. Rev. C **79**, 044906 (2009)
29. B.L. Combridge, Nucl. Phys. B **151**, 429 (1979)
30. S. Frixione, P. Nason, G. Ridolfi, arXiv:0707.3081 [hep-ph]
31. S. Frixione, P. Nason, G. Ridolfi, J. High Energy Phys. **0709**, 126 (2007)
32. P.F. Kolb, J. Sollfrank, U. Heinz, Phys. Rev. C **62**, 054909 (2000)
33. P.F. Kolb, R. Rapp, Phys. Rev. C **67**, 044903 (2003)
34. P.F. Kolb, U. Heinz, arXiv:nucl-th/0305084
35. P. Romatschke, U. Romatschke, Phys. Rev. Lett. **99**, 172301 (2007)
36. M. Luzum, P. Romatschke, Phys. Rev. C **78**, 034915 (2008)
37. M. Luzum, P. Romatschke, Phys. Rev. Lett. **103**, 262302 (2009)
38. W.M. Alberico, A. Beraudo, A. De Pace, A. Molinari, M. Monteno, M. Nardi, F. Prino, arXiv:1007.4170 [hep-ph]; arXiv:1009.2434 [hep-ph]; arXiv:1011.0400 [hep-ph]
39. K.J. Eskola, H. Paukkunen, C.A. Salgado, J. High Energy Phys. **0904**, 065 (2009)
40. M. Cacciari, P. Nason, R. Vogt, Phys. Rev. Lett. **95**, 122001 (2005)
41. R. Vogt, Int. J. Mod. Phys. E **12**, 211 (2003)
42. A. Adare et al. (PHENIX Collaboration), Phys. Rev. Lett. **97**, 252002 (2006)
43. B. Alessandro et al. (ALICE Collaboration), J. Phys. G **32**, 1295 (2006)
44. J. Hüfner, Y. Kurihara, H.J. Pirner, Phys. Lett. B **215**, 218 (1988)

45. J. Hüfner, P. Zhuang, Phys. Lett. B **515**, 115 (2001); **559**, 193 (2003)
46. M.C. Abreu *et al.* (NA50 Collaboration), Phys. Lett. B **499**, 85 (2001)
47. H. De Vries, C.W. De Jager, C. De Vries, Atom. Data Nucl. Data Tabl. **36**, 495 (1987)
48. M. Laine, Y. Schroder, Phys. Rev. D **73**, 085009 (2006)
49. K. Aamodt et al. (ALICE collaboration), arXiv:1011.3916 [nucl-ex]
50. G. Kestin, U. Heinz, in *Heavy Ion Collisions at the LHC-Last Call for Predictions*, J. Phys. G **35**, 054001 (2008)
51. R. Chatterjee, E. Frodermann, U. Heinz, D.K. Srivastava, in *Heavy Ion Collisions at the LHC-Last Call for Predictions*, J. Phys. G **35**, 054001 (2008)
52. P. Kloeden, E. Platen, *Numerical Solution of Stochastic Differential Equations*, (Springer, Heidelberg, 2000)
53. A.W.C. Lau, T.C. Lubensky, Phys. Rev. E **76**, 011123 (2007)
54. O.Kaczmarek, F. Zantow, Phys. Rev. D **71**, 114510 (2005)
55. S. Chekanov et al. (ZEUS Collaboration), Eur. Phys. J. C **44**, 351 (2005)
56. http://www.slac.stanford.edu/xorg/hfag/osc/PDG_2009/
57. C. Peterson, D. Schlatter, I. Schmitt, P.M. Zerwas, Phys. Rev. D **27**, 105 (1983)
58. E. Braaten, K. Cheung, S. Fleming, T.C. Yuan, Phys. Rev. D **51**, 4819 (1995) 4819.
59. T. Sjostrand, S. Mrenna, P.Z. Skands, J. High Energy Phys. **0605**, 026 (2006)
60. K. Nakamura et al. (Particle Data Group), J. Phys. G **37**, 075021 (2010)
61. D.G. d'Enterria, arXiv: nucl-ex/0302016
62. R.L. Thews, M.L. Mangano, Phys. Rev. C **73**, 014904 (2006)